Original article

MOLECULAR METABOLISM

Metabolic reprogramming through fatty acid transport protein 1 (FATP1) regulates macrophage inflammatory potential and adipose inflammation

Amy R. Johnson [1,13], Yuanyuan Qin [1,13], Alyssa J. Cozzo [1], Alex J. Freemerman [1], Megan J. Huang [1], Liyang Zhao [1], Brante P. Sampey [1,14], J. Justin Milner [1,15], Melinda A. Beck [1,2,6], Blossom Damania [3,5], Naim Rashid [4,5], Joseph A. Galanko [2,6], Douglas P. Lee [7], Matthew L. Edin [8], Darryl C. Zeldin [8], Patrick T. Fueger [9,10], Brittney Dietz [11], Andreas Stahl [11], Ying Wu [12], Karen L. Mohlke [12], Liza Makowski [1,2,5,6,*]

ABSTRACT

Objective: A novel approach to regulate obesity-associated adipose inflammation may be through metabolic reprogramming of macrophages (MΦs). Broadly speaking, MΦs dependent on glucose are pro-inflammatory, classically activated MΦs (CAM), which contribute to adipose inflammation and insulin resistance. In contrast, MΦs that primarily metabolize fatty acids are alternatively activated MΦs (AAM) and maintain tissue insulin sensitivity. In actuality, there is much flexibility and overlap in the CAM-AAM spectrum *in vivo* dependent upon various stimuli in the microenvironment. We hypothesized that specific lipid trafficking proteins, e.g. fatty acid transport protein 1 (FATP1), would direct MΦ fatty acid transport and metabolism to limit inflammation and contribute to the maintenance of adipose tissue homeostasis.

Methods: Bone marrow derived MΦs (BMDMs) from *Fatp1*$^{-/-}$ and *Fatp1*$^{+/+}$ mice were used to investigate FATP1-dependent substrate metabolism, bioenergetics, metabolomics, and inflammatory responses. We also generated C57BL/6J chimeric mice by bone marrow transplant specifically lacking hematopoetic FATP1 (*Fatp1*$^{B-/-}$) and controls *Fatp1*$^{B+/+}$. Mice were challenged by high fat diet (HFD) or low fat diet (LFD) and analyses including MRI, glucose and insulin tolerance tests, flow cytometric, histologic, and protein quantification assays were conducted. Finally, an FATP1-overexpressing RAW 264.7 MΦ cell line (FATP1-OE) and empty vector control (FATP1-EV) were developed as a gain of function model to test effects on substrate metabolism, bioenergetics, metabolomics, and inflammatory responses.

Results: *Fatp1* is downregulated with pro-inflammatory stimulation of MΦs. *Fatp1*$^{-/-}$ BMDMs and FATP1-OE RAW 264.7 MΦs demonstrated that FATP1 reciprocally controled metabolic flexibility, i.e. lipid and glucose metabolism, which was associated with inflammatory response. Supporting our previous work demonstrating the positive relationship between glucose metabolism and inflammation, loss of FATP1 enhanced glucose metabolism and exaggerated the pro-inflammatory CAM phenotype. *Fatp1*$^{B-/-}$ chimeras fed a HFD gained more epididymal white adipose mass, which was inflamed and oxidatively stressed, compared to HFD-fed *Fatp1*$^{B+/+}$ controls. Adipose tissue macrophages displayed a CAM-like phenotype in the absence of *Fatp1*. Conversely, functional overexpression of FATP1 decreased many aspects of glucose metabolism and diminished CAM-stimulated inflammation *in vitro*. FATP1 displayed acyl-CoA synthetase activity for long chain fatty acids in MΦs and modulated lipid mediator metabolism in MΦs.

[1]Department of Nutrition, Gillings School of Global Public Health, University of North Carolina at Chapel Hill, Chapel Hill, NC 27599, USA [2]Department of Nutrition, School of Medicine, University of North Carolina at Chapel Hill, Chapel Hill, NC 27599, USA [3]Department of Microbiology and Immunology, University of North Carolina at Chapel Hill, Chapel Hill, NC 27599, USA [4]Department of Biostatistics, University of North Carolina at Chapel Hill, Chapel Hill, NC 27599, USA [5]Lineberger Comprehensive Cancer Center, University of North Carolina at Chapel Hill, Chapel Hill, NC 27599, USA [6]Nutrition Obesity Research Center, University of North Carolina at Chapel Hill, Chapel Hill, NC 27599, USA [7]Omic Insight, Inc., Durham, NC 27713, USA [8]Division of Intramural Research, National Institute of Environmental Health Sciences, Research Triangle Park, NC 27709, USA [9]Departments of Pediatrics, Indiana University School of Medicine, Indianapolis, IN 46202, USA [10]Departments of Cellular and Integrative Physiology, Indiana University School of Medicine, Indianapolis, IN 46202, USA [11]Department of Nutritional Sciences and Toxicology, University of California Berkeley, Berkeley, CA 94720, USA [12]Department of Genetics, University of North Carolina at Chapel Hill, Chapel Hill, NC 27599, USA

[13] Co-first authors.

[14] Current affiliation: Roivant Sciences, Inc. Roviant, NC, 27701, USA.

[15] Current affiliation: Division of Biological Sciences, University of California San Diego, La Jolla, CA, 92093, USA.

*Corresponding author. CB7461, Department of Nutrition, University of North Carolina at Chapel Hill, Chapel Hill, NC 27599, USA. E-mail: liza.makowski@unc.edu (L. Makowski).

Received March 20, 2016 • Revision received April 8, 2016 • Accepted April 18, 2016 • Available online 23 April 2016

http://dx.doi.org/10.1016/j.molmet.2016.04.005

Conclusion: Our findings provide evidence that FATP1 is a novel regulator of MΦ activation through control of substrate metabolism. Absence of FATP1 exacerbated pro-inflammatory activation *in vitro* and increased local and systemic components of the metabolic syndrome in HFD-fed *Fatp1*$^{B-/-}$ mice. In contrast, gain of FATP1 activity in MΦs suggested that *Fatp1*-mediated activation of fatty acids, substrate switch to glucose, oxidative stress, and lipid mediator synthesis are potential mechanisms. We demonstrate for the first time that FATP1 provides a unique mechanism by which the inflammatory tone of adipose and systemic metabolism may be regulated.

Keywords Adipose tissue macrophage; M2 macrophage; Obesity; Glycolysis; Crown-like structures; Mitochondria

Abbreviations

9-HODE	9-hydroxy-10,12-octadecadienoic acid
AAM	Alternatively activated macrophage
ACK	Ammonium-Chloride-Potassium
ACSL	Long chain acyl-CoA synthetase
ATM	Adipose tissue macrophage
BMDM	Bone marrow derived macrophage
BMT	Bone marrow transplant
BSA	Bovine serum albumin
CAM	Classically activated macrophage
CDP-choline	Cytidine diphosphate-choline
CLS	crown-like structures
CoA	coenzyme A
DMEM	Eagle's minimal essential medium
ECAR	Extracellular acidification rate
eQTLs	Expression quantitative trait loci
eWAT	Epididymal white adipose tissue
FATP1	Fatty acid transport protein 1
FATP1-EV	FATP1- empty vector
FATP1-OE	FATP1- over-expresser
GLUT1	Glucose transporter 1
GTT	Glucose tolerance test
HFD	High fat diet
Hmox-1	Heme oxygenase − 1
$HOMA_{IR}$	Homeostasis model assessment of insulin resistance
IFNγ	Interferon gamma
IL-1β	Interleukin 1β
IL-4	Interleukin 4
IL-6	Interleukin 6
iNOS	Inducible nitric oxide synthase
ITT	Insulin tolerance test
Lamp2	Lysosome-associated membrane protein 2
LCFA	Long chain fatty acids
LFD	Low fat diet
Lipa	Lipase A
LPS	Lipopolysaccharide
MΦ	Macrophage
MCP-1	Monocyte chemoattractant protein-1
METSIM	The METabolic Syndromes In Men
MTT	3-(4, 5-dimethylthiazolyl-2)-2,5-diphenyltetrazolium bromide
MuTHER	The Multiple Tissue Human Expression Resource
NADPH	Nicotinamide adenine dinucleotide phosphate
NLRP3	NLR family, pyrin domain containing 3
OCR	Oxygen consumption rate
$PGF_{2\alpha}$	Prostaglandin F2 alpha
PPARγ	Peroxisome proliferator-activated receptor gamma
PPP	Pentose phosphate pathway
PRPP	phosphoribosyl pyrophosphate
Pycard	Apoptosis-associated speck-like protein containing a CARD
SAM	S-adenosylmethionine
SVF	Stroma vascular fraction
TLR4	Toll-like receptor 4
TNF-α	Tumor necrosis factor alpha

1. INTRODUCTION

Chronic over-nutrition results in low-grade inflammation in metabolically sensitive tissues that contributes to systemic metabolic dysregulation. In obese individuals, as much as 40% of total body composition is adipose. Adipose tissue MΦs (ATMs) may account for up to 50% of the cellularity in the obese adipose microenvironment compared to just 10–20% in non-obese [1,2], demonstrating that ATMs play a central role in shaping the adipose inflammatory milieu. Indeed, ATMs are the primary source of inflammatory cytokines such as tumor necrosis factor alpha (TNF-α) and interleukin 6 (IL-6) in adipose tissue, and, thus, perpetuate obesity-associated inflammation and subsequent comorbidities. Adipose inflammation in obesity has been linked to insulin resistance, type 2 diabetes, cardiovascular disease, and cancer [3,4]. Understanding the etiology of metabolic associated inflammation is critical for combating metabolic diseases. Dramatic changes within the adipose microenvironment occur with the onset and progression of obesity, including an influx of monocytes [5]. Initial studies in the early 2000s described dichotomous ATM phenotypes, either pro- or anti-inflammatory [6]. Several models suggested that monocytes differentiate into pro-inflammatory, or "classically activated" MΦs (CAM), in response to the conditions encountered within the obese adipose microenvironment. Persistent CAM activation is purported to sustain adipose inflammation, eventually leading to impaired function of this tissue [4,7,8]. Resident anti-inflammatory MΦs (AAM), also termed "alternatively activated", are recognized to maintain tissue homeostasis, including insulin sensitivity, by supporting remodeling and secretion of anti-inflammatory cytokines [4]. *In vitro*, CAMs are modeled by activation of the so-called "M1" classical pathway upon exposure to type 1 T-helper cytokines [9]. In contrast, AAMs are activated to the "M2" phenotype by exposure to type 2 T-helper cytokines *in vitro* [6]. Recent evidence also has suggested that in both obesity and weight loss, ATMs can be "metabolically" activated and direct lipid trafficking, thus buffering against the excessive free fatty acid concentrations resulting from enhanced lipolysis in adipose [10–12]. These MΦs are characterized by expression of both CAM- and AAM-associated surface markers, enhanced lysosome biogenesis, expression of PPARγ responsive genes and inhibited autophagy [10,11].

As appreciation of the complexity of the ATM inflammatory phenotype has evolved, so has understanding of the metabolic signature associated with ATMs [13–15]. We and others have demonstrated that CAMs exhibit a significant up-regulation of glucose metabolism, particularly flux through the pentose phosphate pathway (PPP) to generate reactive oxygen species (ROS) [16–19]. We reported that pro-inflammatory activation is achievable by enhancing glucose metabolism via glucose transporter 1 (GLUT1) overexpression using an *in vitro* model, even in the absence of external stimuli [20], in a

demonstration of the tight immunometabolic link between MΦ metabolic reprogramming and activation state. As second messengers, ROS drive production of inflammatory enzymes, cytokines, and chemokines such as inducible nitric oxide synthase (iNOS), TNF-α, monocyte chemoattractant protein-1 (MCP-1) and IL-6 [4,16]. Overall, when considering metabolic phenotype of MΦs, CAMs are primarily glucose-dependent. In contrast, lysosomal lipolysis and fatty acid oxidative metabolism is necessary to generate AAMs [11,12,18,21], although other CPT1-mediated functions may also be important [22]. In a clear link between the immune response and metabolism, iNOS production of nitric oxide (NO) is a key mediator promoting the glycolytic/pro-inflammatory phenotype of MΦs and blunting the anti-inflammatory phenotype through NO's role in inhibiting the electron transport chain associated with oxidative metabolism in AAM [23]. Thus, it is clear that while our understanding of MΦ markers, function and immune response has increased, the complexity of metabolism in regulating MΦ biology — especially in changing *in vivo* microenvironments — remains uncertain.

Metabolic reprogramming of MΦs offers a novel means of regulating inflammation, hence we hypothesized that metabolism of fatty acids by specific lipid trafficking proteins plays a critical role in suppressing ATM-mediated inflammation and maintaining glucose tolerance. Fatty acid transport protein 1 (FATP1, SLC27A1) is an ideal candidate for limiting pro-inflammatory activation: FATP1 is an acyl-CoA synthetase with affinity for long and very long chain fatty acids [24] — lending specificity to its function — which is important because some MΦ fatty acid transporters, such as CD36, are promiscuous [21,25]. FATP1 expression levels are highest in tissues characterized by active fatty acid uptake and lipid metabolism, such as adipose, heart, and skeletal muscle and is primarily localized to the plasma membrane, mitochondria, and peroxisomes [26–28]. In adipocytes, FATP1 activity is regulated by insulin-mediated translocation that increases fatty acid uptake [29]. Studies of total-body *Fatp1* knockout mice demonstrated that loss of FATP1 protected mice from the effects of HFD-induced obesity, insulin resistance, and intramuscular lipid accumulation [29,30]. Functional characterization of FATP1 and activation of fatty acids through its ACSL activity have been conducted in these tissues and cell types, but, to date, not in MΦs [29–34]. Due to its complex expression pattern, the contribution of FATP1 to the development of insulin resistance is likely to be tissue- and cell-type specific. *In silico* analysis of existing Immunological Genome "ImmGen" Project expression data suggested that *Fatp1* is detected in MΦs and plasmacytoid dendritic cells [35], but not other cells that may contribute to inflammation including monocytes, microglia, B cells, T cells, neutrophils, and eosinophils.

Herein, we report that FATP1 plays a critical role in suppressing inflammation *in vitro* and reducing MΦ infiltration and inflammation *in vivo* through modulation of lipid mediators and oxidative stress. We demonstrate for the first time that FATP1 provides a unique mechanism by which the metabolic and inflammatory tone of adipose and systemic metabolism may be regulated.

2. MATERIALS AND METHODS

2.1. Reagents

All reagents were obtained from Sigma–Aldrich (St. Louis, MO) unless otherwise noted. IFNγ and IL-4 were obtained from R&D Systems (Minneapolis, MN). Lipopolysaccharide (LPS, Sigma E. coli L4391) was diluted in sterile PBS at a final concentration of 1 mg/mL. Novolin® human insulin was purchased from Novo Nordisk (Plainsboro, NJ). Antibodies were purchased from the following sources: F4/80 (AbD Serotec/BioRad, Hercules, CA); CD16/32 (Fc Block, BioLegend, San Diego, CA), CD45-FITC, F4/80-PE, Ly6G/C-PE-Cy7, CD11b-APC, CD11c-APC-eFluor 780, CD11c-eFluor 450, CD206-APC (eBioscience, San Diego, CA), PhosphoAKT-Ser473 and total AKT (Cell Signaling Technology), and insulin (H-86; Santa Cruz Biotechnology, Inc., Santa Cruz, CA).

2.2. Animals and diets

Animal studies were performed with approval and in accordance with the guidelines of the Institutional Animal Care and Use Committee at the University of North Carolina at Chapel Hill. Animals were cared for according to the recommendations of the Panel on Euthanasia of the American Veterinary Medical Association. The veterinary care provided at UNC is in compliance with the Public Health Service Policy on Humane Care and Use of Laboratory Animals and meets the National Institutes of Health standards as set forth in the Guide for the Care and Use of Laboratory Animals (DHHS Publication No. (NIH) 85-23 Revised 1985). The animal facility is Association for Assessment and Accreditation of Laboratory Animal Care (AAALAC) approved and is responsible for the health and husbandry of animals. UNC also accepts as mandatory the PHS Policy on Humane Care and Use of Laboratory Animals be Awardee Institutions and NIH Principles for the Utilization and Care of Vertebrate Animals Used in Testing, Research, and Training. Animal studies comply with the ARRIVE guidelines. Mice were housed in a climate controlled Department of Laboratory Animal Medicine facility with a 12-hour light:dark cycle and *ad libitum* access to food and water. *Fatp1*$^{-/-}$ mice [30] were backcrossed >12 generations to the C57BL/6J genetic background. *Fatp1* total body knockout (*Fatp1*$^{-/-}$) and *Fatp1* wild type (*Fatp1*$^{+/+}$) bone marrow donor mice were generated using *Fatp1*$^{-/+}$ breeding pairs to generate littermate controls.

2.3. Adipose tissue MΦs

To isolate ATMs from lean and obese adipose, male C57BL/6J mice were randomized onto either chow or an obesogenic diet (HFD, 45% kcal from fat, HFD; D06011802, Research Diets, New Brunswick, NJ) at weaning. After 23 weeks on diet, epididymal white adipose tissue (eWAT) was minced in 25 mM HEPES-buffered DMEM/1% fatty acid-free, low endotoxin BSA (Sigma) and completely digested with 0.5 mg/mL Liberase TM (Roche Diagnostics, Indianapolis, IN) at 37°. Samples were centrifuged at 200× *g* for 10 min at 4° to pellet the MΦ-rich stroma vascular fraction (SVF). The pellet was washed twice with in 25 mM HEPES-buffered DMEM/1% fatty acid-free, low endotoxin BSA and red blood cells were lysed and washed again. Samples were stained with anti-F4/80-PE and sorted on a MoFlo cell sorter (Beckman Coulter, Brea, CA). F4/80^{hi} MΦs were collected for mRNA isolation and gene expression analysis.

2.4. *Fatp1* genotyping

Genomic DNA was isolated from tail biopsies, eWAT, and BMDM using a DNeasy Blood and Tissue kit (Qiagen, Valencia, CA). Genotyping was performed using the following primers: *Fatp1* forward: GGCGGT CAATGTTAAGTAAACTGG, *Fatp1*$^{+/+}$ reverse: CTCACACCACCCTGCAAGACTCT, *Fatp1*$^{-/-}$ neomycin cassette reverse: GTAATGGGATAGGT CACGTTGGTG [30]. iProof High-Fidelity PCR super mix (Bio-Rad, Hercules, CA)-based genotyping was performed on a C1000 thermocycler (Bio-Rad, Hercules, CA).

2.5. BMDM isolation, differentiation, and activation

Bone marrow was collected from chow-fed gender- and age-matched male *Fatp1*$^{+/+}$ and *Fatp1*$^{-/-}$ mice. Marrow was cultured in RPMI-

1640 containing 30% L929 conditioned media supplemented with 10% FBS, 2 mM glutamine, 100 IU/mL penicillin and 100 μg/mL streptomycin (Sigma–Aldrich, St. Louis, MO). For bioenergetics assays, BMDM were differentiated using M-CSF (20 ng/ml). BMDM were left as naïve unstimulated MΦs (Un), or activated using 5 ng/mL LPS and 10 ng/mL IFNγ (CAM) or 10 ng/mL IL-4 (AAM) for 24 h [18]. Cell densities and viability were determined by hematocytometer and trypan blue exclusion, respectively. Cell size, volume, and viability were determined using a Sceptor™ handheld automated cell counter (Millipore, Billerica, MA).

2.6. Immunoblot

FATP1 protein expression was measured by immunoblotting as previously described [36]. Polyclonal anti-sera raised against the C-terminus of FATP1 or antibody against β-tubulin diluted 1:1000 in PBS with 0.1% Tween-20, overnight was used. Primary antibodies were detected with LI-COR secondary antibodies and imaged on the LI-COR Odyssey Imaging System (Lincoln, NE). PhosphoAKT (ser473) and total AKT was measured by immunoblotting as previously described [37].

2.7. Long chain acyl-CoA synthetase (ACSL) activity assay

Total ACSL activity was measured as previously described [38]. ^{14}C-Oleate acid (PerkinElmer Life Sciences, Akron, OH) was incubated with cell homogenate and reactions were terminated after 10 min. Heptane-washed aqueous phase (0.6 mL) was counted on a Wallac 1409 Liquid scintillation counter (PerkinElmer Life Science, Waltham, MA). Total ACSL activity was expressed as nanomoles of oleate-CoA ester formed/minute/mg protein.

2.8. Metabolomics and eicosanoid profiling

Fatp1$^{+/+}$ and *Fatp1*$^{-/-}$ BMDM or FATP1-EV and FATP1-OE RAW264.7 were plated on low binding, non-tissue culture treated plates. 24 h after plating, both RAW MΦs and BMDM were left untreated (Un) or activated to CAM as above. Analysis of AAM-stimulated MΦs at Metabolon were cost prohibitive at the time of this study. PBS-washed cells were detached by scraping, flash frozen in liquid nitrogen, and metabolomics analysis on lysates was completed by Metabolon, Inc. (Research Triangle Park, NC) [39]. N = 4 replicates per group. Missing values were imputed with the minimum. Data are presented as relative measures of "scaled intensity" after normalization to protein and median scaling to 1. For measurement of eWAT 8-iso-PGF$_{2\alpha}$ and cell media eicosanoids, lipids were extracted from 25 mg of pulverized eWAT tissue and eicosanoids were quantified by liquid chromatography with an Agilent 1200 Series capillary HPLC (Agilent Technologies, Santa Clara, CA, USA) as previously described [40]. Negative ion electrospray ionization tandem mass spectrometry was used for detection. N = 8 per group for eWAT and N = 4 for cell media from *Fatp1*$^{+/+}$ and *Fatp1*$^{-/-}$ BMDM or FATP1-EV and FATP1-OE RAW264.7.

2.9. High fat diet study

MΦ *Fatp1*$^{+/+}$ (*Fatp1*$^{bonemarrow+/+}$, *Fatp1*$^{B+/+}$) and deficient (*Fatp1*$^{B-/-}$) chimeric mice were generated using bone marrow transplant (BMT) strategy as outlined in supplemental Figure appendix ("A") A5 B. Briefly, 3-week-old male C57BL/6J recipient mice were purchased from Jackson Laboratories (Bar Harbor, ME). Upon arrival, C57BL/6J mice were randomized to either a purified low fat diet (10% kcal from fat, LFD; D07010502, Research Diets, New Brunswick, NJ) or HFD. At 6 weeks of age, recipient mice were administered 2 doses of X-ray radiation (500 cGy × 2, spaced 4 h apart; X-RAD, North Branford, CT). Simultaneously, bone marrow was harvested from 6 week old male *Fatp1*$^{-/-}$ and *Fatp1*$^{+/+}$ donor mice maintained on standard chow and transplanted as in Makowski et al. [41]. Control irradiated animals that were not reconstituted with bone marrow died within 10 days of irradiation. *Fatp1*$^{B+/+}$and *Fatp1*$^{B-/-}$ chimeric animals were maintained on LFD or HFD for a total of 23 weeks. N = 16–17 mice per diet group and genotype.

2.10. Metabolic phenotyping

Body composition was measured immediately prior to BMT and prior to sacrifice (at 23 weeks on diet) using magnetic resonance imaging (MRI, EchoMRI, Houston, TX). Blood glucose was measured at 3 weeks on the diets and again at termination, both following a 6 h fast. Randomly fed blood glucose was measured at 9:00 AM after 23 weeks on diet. Intraperitoneal glucose tolerance tests (GTT) and insulin tolerance tests (ITT) were performed at weeks 19 and 20 on diet, following 6 or 4 h fast, respectively [42]. Briefly, 2.0 gm/kg body weight of glucose or 0.75U of insulin was injected intraperitoneally, and blood glucose was measured over 120 min. All blood glucose measurements were performed using a FreeStyle Freedom Lite glucometer (Abbot Diabetes Care, Inc., Alameda, CA). Plasma insulin was measured by ELISA (EMD Millipore, Billerica, MA). Fasting glucose (mg/dL) and insulin (pmol/L) concentrations measured just prior to euthanasia were used to calculate HOMA$_{IR}$ and HOMA$_{\%B}$ [43]. N = 5 mice were injected with insulin (0.75 U) prior to euthanasia in 6 h fasted mice to determine insulin sensitivity by Western Immunoblot.

2.11. Tissue and blood collection

Animals were euthanized with tribromoethanol/amylene hydrate (1.25%, Sigma Aldrich, St. Louis, MO). Blood was collected via cardiac puncture and plasma was separated from other blood components by centrifugation at 200× *g* for 5 min at 4 °C. eWAT and pancreata were collected and fixed in 10% formalin for histological analyses. A portion of eWAT tissue was flash frozen and pulverized in liquid nitrogen for Western immunoblot.

2.12. Hematologic analysis

Hematologic analysis was conducted on fed 10-week-old *Fatp1*$^{+/+}$ and *Fatp1*$^{-/-}$ age-matched male and female mice maintained on *ad libitum* chow. Blood was collected by submandibular bleed into EDTA-coated tubes. Hematologic analysis occurred in the UNC Mouse Clinical Chemistry Core using an automated hematology analyzer. In addition, flow cytometry was used to enumerate circulating leukocyte populations. Blood was collected from samples for hematologic analysis, and red blood cells were lysed in ACK lysis buffer. Cells were washed twice in HBSS, resuspended in PBS, counted, and then 1 × 10^5 cells were stained with CD45-FITC, F4/80-PE, Ly6G/C-PE-Cy7, CD11b-APC, CD11c-APC-eFluor 780 in the presence of anti-CD16/32 (Fc block) in FACS buffer (1% FBS in PBS) as described in Murphy et al. [44]. Samples were analyzed on the Dako CyAN ADP flow cytometer (Beckman Coulter, Inc., Fullerton, CA) and FlowJo Software (TreeStar, Ashland, OR). Gating strategy is included as supplemental Figure A1.

2.13. Quantitation of secreted cytokines and chemokines

Concentrations of plasma leptin, IL-6, TNFα, and MCP-1 or conditioned media IL-1β, IL-6, Il-10, and MCP-1 were measured using a MAGPIX Luminex kit (EMD Millipore, Billerica, MA).

2.14. Gene expression analysis

Total mRNA was isolated from eWAT and cultured cells using an RNeasy kit (Qiagen, Valencia, CA). RNA quantity and quality was

determined using Nanodrop (ThermoScientfic, Wilmington, DE) and reverse transcribed using the iScript cDNA synthesis kit (Bio-Rad, Hercules, CA). Gene expression was quantitated by qPCR using Assay-On-Demand chemistries on an ABI 7900HT machine (Life Technologies, Grand Island, NY) [45]. Expression levels of genes of interest were normalized to expression of *18S*. Animals whose body weight was at or above the mean body weight for the experimental group were selected for analysis; therefore, unless indicated, N = 8–9/group for mouse data and N = 3–6 experiments for cell culture studies.

2.15. Morphological and immunohistochemical analyses of eWAT and pancreata

Anti-F4/80 and 4-HNE immunohistochemistry staining was conducted as previously described [46]. Pancreatic islets of Langerhans were visualized by H&E [46,47]. All histological sections were scanned on an Aperio ScanScope CS Ultra-Resolution Digital Scanner and analyzed using ScanScope Image Analysis Toolbox software (Buffalo Grove, IL) [37].

2.16. FATP1-OE stable MΦ cell line generation and characterization

The DNA sequence for *Fatp1* was obtained from the National Institutes of Health Mammalian Gene Collection. *Fatp1* cDNA containing a 5′ *EcoRI* site followed by a Kozak sequence and Flag tag and a 3′ *NotI* site was cloned into the pCI-neo Mammalian Expression vector (Promega, Madison, WI). The upstream primer: 5′-GATCGAATTCGCCACCATGGATTACAAGGATGACGACGATAAGCGGGCTCCTGGAGCAGGAACAGCC-3'. The down stream primer: 5′-GATCGCGGCCGCTCAGAGTGAGAAGTCGCCTGC-3'. Sequencing confirmed the fidelity of the sequence. Mouse RAW264.7 MΦ cells (ATCC, Manassas, VA; ATCC# TIB-71) were transfected with either the empty vector (FATP1-EV) or FATP1 expression construct (FATP1-OE) using the AMAXA Nucleofector V kit (Lonza, Cologne, Germany). Stable cell lines were established and diluted serially to obtain clonal isolates under selection using 400 μg/ml G418 Sulfate (Cellgro, Manassas, VA) for 2 weeks. All transfected MΦs were subsequently maintained in 200 μg/mL G418 Sulfate. RAW264.7 FATP1-EV and FATP1-OE cells were grown in Dulbecco's minimal essential media (DMEM) 4.5 g/L glucose supplemented with 10% FBS, 100 IU/mL penicillin and 100 μg/mL streptomycin (Sigma–Aldrich, St. Louis, MO). Studies reported herein were repeated in a second set of clones and the parent heterologous population of FATP-EV and FATP1-OE from which the clones were isolated (data not shown). Cell viability, size and volume were determined as above. Cell proliferation was determined by 3-(4, 5-dimethylthiazolyl-2)-2,5-diphenyltetrazolium bromide (MTT) assay (ATCC) over 24–96 h of culture [20].

2.17. Substrate uptake and metabolism

FATP1-EV and FATP1-OE RAW264.7, or $Fatp1^{+/+}$ and $Fatp1^{-/-}$ BMDM were plated at 1.5×10^5 or 7.5×10^5 cells/well, respectively, into 24 well plates, allowed to attach overnight and stimulated as above. Cells were washed with PBS and then incubated untreated or with 2 μM BODIPY® C_{16} fluorescent palmitic acid (Molecular Probe, Grand Island, NY) in DMEM for 30 min at 37 °C [48]. Fluorescence was measured using a CyAn ADP Analyzer flow cytometer (Beckman Coulter, Fullerton, CA) and FlowJo software (TreeStar, Ashland, OR) [49]. To measure fatty acid oxidation, 1.0 μCi/mL BSA-conjugated 1-[^{14}C]-oleic acid (PerkinElmer Life Sciences, Waltham, MA) was added to DMEM containing 12.5 mM HEPES, 1 mM L-carnitine to a final concentration of 0.5%, 100 μM sodium oleate. ^{14}C-CO_2 was captured and counted using EcoScint H. Glucose uptake, oxidation and glycogen synthesis were measured as previously described [20]. Results were normalized to protein concentration.

2.18. Cellular bioenergetics

FATP1-EV or FATP1-OE RAW MΦs (6×10^4/well) were seeded into a Seahorse Bioscience (Billerica, MA) tissue culture plate, allowed to attach for 3 h and activated with 100 ng/mL LPS (RAW264.7) or PBS vehicle control. $Fatp1^{+/+}$ or $Fatp1^{-/-}$ BMDMs (2×10^5/well) were seeded and allowed to attach for 3 h and then either left as naïve unstimulated MΦs (Un), CAM, or AAM activated for 24 h as above. Prior to analysis, cells were washed twice with DMEM (RAW) or RPMI (BMDM) assay media (sodium bicarbonate- and glucose-free DMEM or RPMI supplemented with 2 mM glutamine, 100 IU/mL penicillin and 100 μg/mL streptomycin (Sigma–Aldrich, St. Louis, MO) and equilibrated for 1 h at 37 °C without CO_2. Measures of glycolytic rate and glycolytic capacity were determined by recording extracellular acidification rates (ECAR, mpH/min) and oxygen consumption rates (OCR, pmol/min) on a Seahorse Bioscience XF24 Extracellular Flux Analyzer (Billerica, MA) [50]. The injection of glucose was used to measure glycolytic rate (final concentration 25 mM (RAW) or 11 mM (BMDM); Sigma, St. Louis, MO). Oligomycin was injected to measure glycolytic capacity (final concentration 2.5 μM; Sigma, St. Louis, MO). 2-deoxyglucose was used to blunt glycolysis (final concentration 20 mM). N = 6 replicates per genotype/treatment. Equal plating density was confirmed by protein assay. Experiments were repeated a minimum of three times.

2.19. Human gene expression, variants, and trait association

To determine whether human genetic variants may act as *cis*-regulators of *FATP1* expression, we searched for expression quantitative trait loci (eQTLs) for *FATP1* (*SLC27A1*) located within 1 Mb of the coding sequence. We searched the Multiple Tissue Human Expression Resource (MuTHER) study of HapMap-imputed variants associated with gene expression in subcutaneous adipose tissue from 856 female twins [51] available in the Genvar database [51]. We used the same criteria to look up *cis*-eQTLs in subcutaneous adipose expression data from the METabolic Syndrome In Men (METSIM) study of 1000 Genomes-imputed variants in 1381 men [52]. Expression levels were analyzed after adjustment for 40 inferred determinants from factor analysis [53].

2.20. Statistics

For body weight data analyses, a regression model was run with genotype/diet group and week (0 thru 23) as predictors. To account for the repeated measures over time within animals an autoregressive within-subject correlation matrix was fit. F-tests using the resulting parameter and standard error estimates were constructed to make comparisons of interest. Analyses were performed using SAS Version 9.3 (SAS Institute, Cary NC). Robust pairwise correlations were determined using Spearman Correlation, utilizing pairwise complete observations when missing data was present. We utilized the "cor.test" function in R to obtain exact p-values testing whether the observed correlations were significantly different from 0. PCA plot was made using ArrayStudio (OmicSoft, Cary, NC). For all other *in vivo*, *ex vivo* or *in vitro* data, statistical differences between experimental groups were determined by two-way ANOVA followed by multiple comparisons tests using statistical software within GraphPad Prism (GraphPad Software, Inc., La Jolla, CA). For *ex vivo* and *in vitro* experiments, representative results are reported; at least N = 3 experiments were conducted with N = 3–6 replicates per assay. All data

MOLECULAR METABOLISM

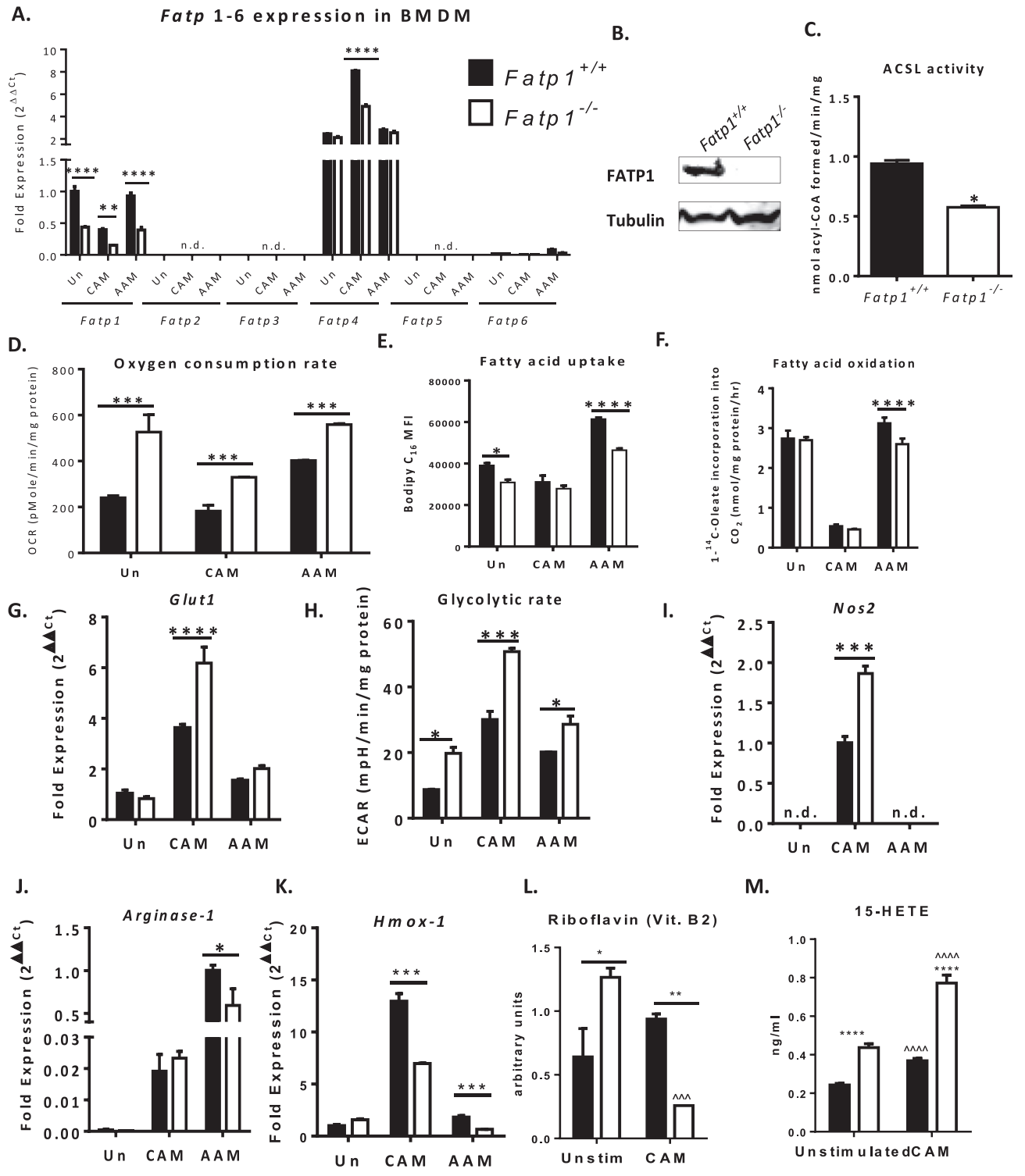

Figure 1: *Fatp1* deletion decreased MΦ acyl-CoA synthetase (ACSL) activity and resulted in a metabolic shift from lipid oxidation to glycolysis that resulted in exacerbated CAM and reduced AAM activation. A. *Fatp1-Fatp6* mRNA was measured in BMDM generated from *Fatp1*$^{+/+}$ and *Fatp1*$^{-/-}$ mice on chow diet (n.d., not detected. **P < 0.01; ****P < 0.0001 *Fatp1*$^{+/+}$ vs. *Fatp1*$^{-/-}$). B. FATP1 protein expression was measured by Western immunoblot in unstimulated BMDM. Tubulin is used as a loading control. C. ACSL activity was measured using ^{14}C—oleate in unstimulated *Fatp1*$^{+/+}$ and *Fatp1*$^{-/-}$ BMDMs (*P < 0.05). D. Oxygen consumption rate (OCR) was measured using the Seahorse Extracellular Flux Analyzer in Un, CAM, and AAM activated BMDM from *Fatp1*$^{+/+}$ and *Fatp1*$^{-/-}$ *mice*. (***P < 0.001). E. Fatty acid uptake was measured using BODIPY®-palmitate (*P < 0.05 and ****P < 0.0001, *Fatp1*$^{+/+}$ vs. *Fatp1*$^{-/-}$). F. Complete fatty acid oxidation was measured using ^{14}C-oleate (*P < 0.0001). G. G*lucose transporter 1* (*Glut1*) mRNA was quantified by qPCR (****P < 0.0001). H. Glycolytic rate, as measured by extracellular acidification rate (ECAR), was measured using the Seahorse Extracellular Flux Analyzer (*P < 0.05, ***P < 0.001). I. *Inducible nitric oxide synthase* (*Nos2*), *Arginase-1* (J) and *Hmox-1* (K) mRNA expression levels were measured by qPCR (*P < 0.05 and ***P < 0.001); activation has an effect in all figures (P < 0.0001). Data are mean ± SEM; differences were detected by two-way ANOVA. Representative of at least N = 3 experiments with n = 4 replicates per experiment. Metabolites including (L) Riboflavin (Vitamin B2) and (M) eicosanoid 15-HETE were quantified (*P < 0.05; **P < 0.01, ***P < 0.001 *Fatp1*$^{+/+}$ vs. *Fatp1*$^{-/-}$ and Ꝑ < 0.001 or Ꝑ < 0.0001 for diet effect, N = 4.).

are shown as mean ± standard error of the mean (SEM). P values less than 0.05 were considered statistically significant.

3. RESULTS

3.1. Lack of FATP1 induced a metabolic substrate switch from fatty acid to glucose metabolism

We hypothesized that FATP1 plays a role in supporting MΦ function and inflammation by directing lipid metabolism in MΦs. To test this hypothesis using a common *in vitro* model to study MΦ biology, BMDM were isolated and differentiated from age-matched, chow-fed male *Fatp1*$^{+/+}$ and *Fatp1*$^{-/-}$ mice. There were no differences in the number or gross morphology of BMDM generated from *Fatp1*$^{-/-}$ mice compared to *Fatp1*$^{+/+}$ mice (data not shown). Figure 1 A shows that in *Fatp1*$^{+/+}$ BMDM, *Fatp1* expression was 2-fold higher in AAM compared to CAM-stimulated BMDMs, replicating *in silico* findings [54]. *Fatp1* expression was reduced ($P < 0.001$) in *Fatp1*$^{-/-}$ BMDM, as expected [30]. *Fatp*2, 3, and 5 were undetected. Relative to *Fatp1*, BMDMs express *Fatp4* at higher concentrations in all activation states. In contrast to *Fatp1, Fatp4* expression is increased 3-fold in CAM activated compared to unstimulated and AAM-stimulated BMDM. No compensation for *Fatp1* deficiency by *Fatp4* or *Fatp6* was detected; in fact, in CAM-stimulated BMDM, *Fatp4* was detected at lower levels in *Fatp1*$^{-/-}$ compared to *Fatp1*$^{+/+}$ BMDM ($P < 0.0001$, Figure 1A). Minor non-translated *Fatp1* mRNA was detected due to where qPCR primers were located. The lack of FATP1 protein (Figure 1B) and a 40% reduction in total ACSL BMDM enzymatic activity ($P < 0.01$, Figure 1C) had no effect on the size or viability of BMDMs (Figure A2 A–B).

To examine effects of lack of FATP1 on MΦ metabolism, we next examined cellular bioenergetics, fatty acid uptake, and substrate metabolism. Mitochondrial oxidative phosphorylation, as measured by oxygen consumption rate (OCR), was elevated in AAMs compared to unstimulated or CAMs, as expected [18]. OCR was significantly higher in *Fatp1*$^{-/-}$ compared to *Fatp1*$^{+/+}$ BMDM in all activation states ($P < 0.001$, Figure 1D). In *Fatp1*$^{+/+}$ BMDM, AAM-activation induced a 57% and 97% increase in fatty acid internalization when compared to unstimulated ($P < 0.0001$) or CAM, respectively ($P < 0.001$, Figure 1E). Compared to *Fatp1*$^{+/+}$, fatty acid uptake was reduced by 21% and 24% in unstimulated ($P < 0.05$) and AAM-activated *Fatp1*$^{-/-}$ BMDM ($P < 0.0001$), respectively. The diminished fatty acid uptake in AAM-activated *Fatp1*$^{-/-}$ BMDM correlated with a 17% reduction in complete oleate oxidation compared to *Fatp1*$^{+/+}$ controls ($P < 0.0001$, Figure 1F). There were no significant differences in incomplete fatty acid oxidation as measured by ^{14}C incorporation into acid soluble metabolites (data not shown).

Because MΦs markedly enhance glucose metabolism when CAM activated, we determined if inhibition of lipid metabolism via deletion of FATP1 would reprogram BMDM metabolism toward increased glucose usage, thus creating a CAM-like metabolic phenotype. Expression of glucose transporter 1 (*Glut1*) was significantly increased in CAM activated *Fatp1*$^{-/-}$ compared to *Fatp1*$^{+/+}$ BMDM ($P < 0.0001$, Figure 1G). Next, extracellular acidification rate (ECAR) was used to measure glycolytic rate. *Fatp1*$^{-/-}$ BMDM displayed significantly increased glycolytic rates in unstimulated ($P < 0.05$), CAM- ($P < 0.001$) and AAM-activated ($P < 0.05$) states compared to *Fatp1*$^{+/+}$ BMDM (Figure 1H). Glycolytic capacity was similarly elevated in the absence of FATP1 (Figure A2 C). Neither glucose oxidation or glycogen synthesis was affected by *Fatp1* genotype (data not shown). Spearman correlation analyses revealed a significant inverse correlation between glycolytic rate and fatty acid oxidation ($r = -0.63$, $P = 3 \times 10^{-4}$). Furthermore, both glycolytic rate ($r = -0.77$, $P = 0.0053$) and capacity ($r = -0.89$, $P = 1 \times 10^{-4}$) were inversely proportional to ACSL activity.

3.2. Lack of FATP1 primed MΦs for exaggerated pro-inflammatory response upon CAM activation and hindered activation to the AAM phenotype

Expanding on our observations that *Fatp1*$^{-/-}$ BMDM internalized and oxidized less fatty acid compared to *Fatp1*$^{+/+}$, together with existing evidence linking MΦ substrate metabolism and inflammatory phenotype [16,18,20], we next measured the basal expression and inflammatory response of *Fatp1*$^{+/+}$ and *Fatp1*$^{-/-}$ BMDMs. Expression of the classic CAM marker inducible nitric oxide synthase (*Nos2*) was 2-fold higher in *Fatp1*$^{-/-}$ compared to *Fatp1*$^{+/+}$ CAM-activated BMDMs ($P < 0.0001$, Figure 1I). AAM marker Arginase-1 (*Arg1*) [18] up-regulation was significantly blunted in *Fatp1*$^{-/-}$ compared to *Fatp1*$^{+/+}$ BMDM ($P < 0.05$, Figure 1J). Furthermore, heme oxygenase − 1 (*Hmox-1*) expression, an anti-inflammatory marker [55,56], was reduced by 50% in both CAM- and AAM-activated *Fatp1*$^{-/-}$ BMDM ($P < 0.001$, Figure 1K). Antigen presenting molecules were also evaluated in BMDM. CD86 and CD80, two molecules that prime T cells, were increased by CAM activation, but regulation was not altered by *Fatp1* (supplemental Figure A3 A–B). HLA class II histocompatibility antigen gamma chain, or CD74, was increased by both CAM and AAM activation, but *Fatp1* did not alter expression significantly (supplemental Figure A3 C).

3.3. Metabolomic analysis of *Fatp1*$^{-/-}$ BMDM indicated enhanced glucose metabolism, particularly through the PPP

To further test FATP1's effects on substrate metabolism, comprehensive metabolomics profiling was undertaken. *Fatp1*$^{+/+}$ and *Fatp1*$^{-/-}$ BMDM were isolated, left unstimulated or CAM activated, and then lysed for metabolite analysis. CAM activation increased 54 and 49 metabolites and downregulated 123 and 115 metabolites in *Fatp1*$^{+/+}$ and *Fatp1*$^{-/-}$, respectively. As expected, carbohydrate metabolism was upregulated with CAM activation of BMDMs regardless of genotype from the unstimulated state especially "Fructose, mannose, galactose, starch, and sucrose metabolism", "Nucleotide sugars, pentose metabolism", and most of the metabolites from glycolysis and the Krebs cycle. However, some metabolites were downregulated with CAM activation including glucose, fumarate, and malate, among others (Table A1, and P values within). Several pathways were also downregulated when BMDMs were CAM activated from the unstimulated state, including the "glycine, serine and threonine metabolism" subpathway, several nucleotides, other amino acid metabolism, dipeptides, and gamma-glutamyl amino acid metabolites. Likewise, most of the cofactor and vitamins were downregulated with the exception of biopterin and two nicotinate and nicotinamide metabolites. There was little regulation of fatty acid metabolism except a decrease in the essential fatty acids docosapentaenoate (n6 DPA; 22:5n6), docosahexaenoate (DHA; 22:6n3), and medium chain fatty acid caproate (6:0) with CAM activation. Increased concentrations of metabolites in glycerolipid metabolism, some lysolipids, and prostaglandins — with a tremendous 40+-fold increase in PGD2 — with CAM stimulation in both genotypes were detected.

We next compared *Fatp1*-directed differences between BMDMs (Table A1, and P values within). Metabolic changes in BMDMs were predominantly driven by CAM activation with overlapping variability in *Fatp1*$^{-/-}$ compared to *Fatp1*$^{+/+}$, as demonstrated by principal component analysis (PCA) plot in supplemental Figure A4. There were a total of 11 metabolites upregulated and 13 downregulated in *Fatp1*$^{-/-}$ compared to *Fatp1*$^{+/+}$ in the inactivated state ($P < 0.05$). When

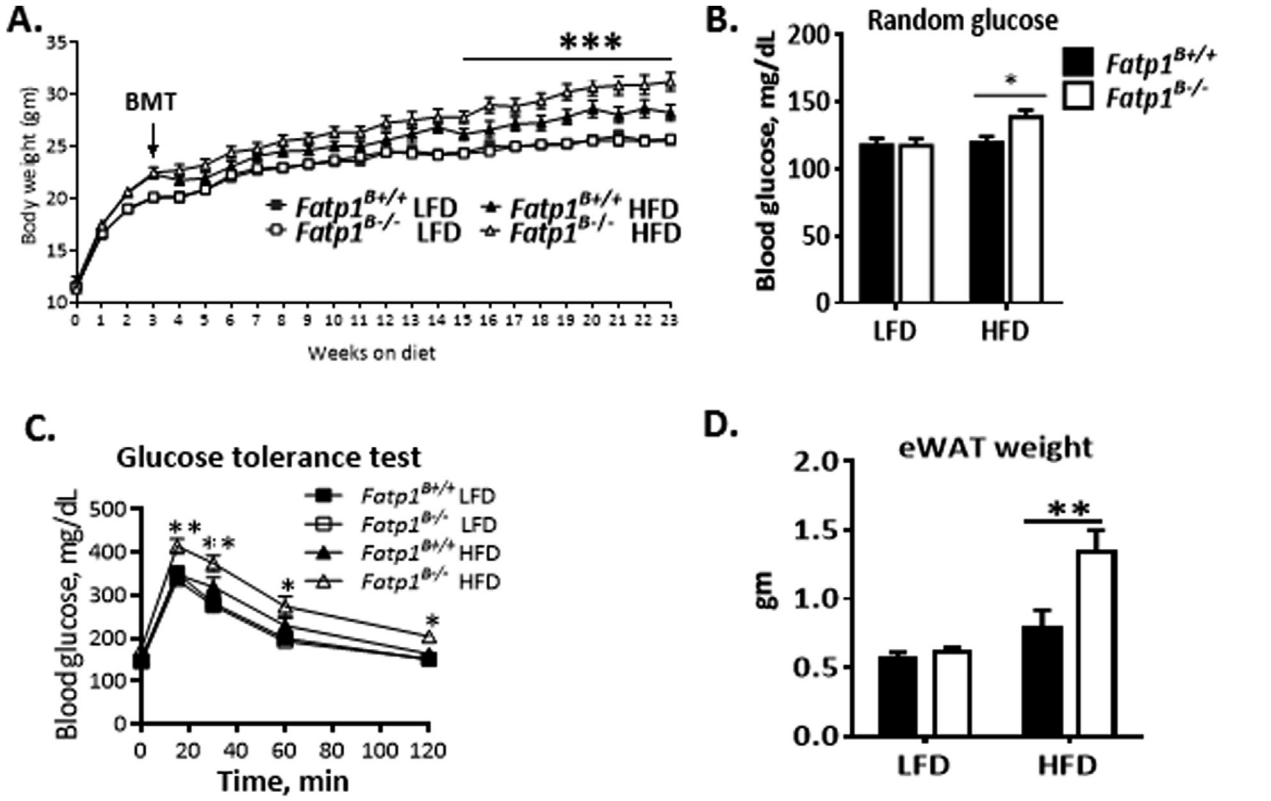

Figure 2: Deletion of MΦ *Fatp1* increased susceptibility to HFD-induced weight gain, glucose intolerance, and increased epididymal white fat mass. A. Body weights were measured weekly ($Fatp1^{B-/-}$ vs. $Fatp1B^{+/+}$ mice on HFD; ***P $<$ 0.001). B. Randomly fed blood glucose was measured at 23 weeks on diet (*P $<$ 0.05). C. Intraperitoneal glucose tolerance tests were conducted at 19 weeks on diet after a 6hr fast. HFD-fed $Fatp1^{B+/+}$ vs. $Fatp1^{B-/-}$ (**P $<$ 0.01 and *P $<$ 0.05). D. Epididymal white fat mass was quantified at sacrifice. In HFD-fed mice, **P $<$ 0.01 in $Fatp1^{B+/+}$ vs. $Fatp1^{B-/-}$ mice. Data are means ± SEM; all differences detected by two-way ANOVA, except for panel "A"; N = 16–17 mice per group which was analyzed by mixed regression modeling.

BMDM were CAM activated, there were 12 upregulated and 13 downregulated in $Fatp1^{-/-}$ compared to $Fatp1^{+/+}$. $Fatp1^{-/-}$ in both unstimulated and CAM activated states had greater concentrations of metabolites including glutamate, hypotaurine, taurine, N-acetylneuraminate, and the medium chain fatty acid pelargonate (9:0). Significantly lower concentrations of some metabolites in the pathways entitled "Fructose, mannose, galactose, starch, and sucrose metabolism", "Glycolysis, gluconeogenesis, pyruvate metabolism" and "Glycine, serine and threonine metabolism" were detected. For example, significantly lower concentrations of sorbitol, glucose, glycine, serine, and asparagine were detected in $Fatp1^{-/-}$ in both unstimulated and CAM activated states compared to $Fatp1^{+/+}$. 22% less intracellular lactate was detected in $Fatp1^{-/-}$ BMDM compared to $Fatp1^{+/+}$ in the CAM-stimulated state. $Fatp1^{-/-}$ displayed significantly less ethanolamine in the unstimulated state compared to $Fatp1^{+/+}$ (P $<$ 0.05), but concentrations between $Fatp1^{+/+}$ and $Fatp1^{-/-}$ were identical in CAM. Riboflavin (or Vitamin B2) was another metabolite that was significantly 1.97-fold greater in $Fatp1^{-/-}$ compared to $Fatp1^{+/+}$ BMDM in the unstimulated state (P $<$ 0.05, Figure 1L) but was significantly lower (0.27-fold or 73% less) in $Fatp1^{-/-}$ BMDMs compared to $Fatp1^{+/+}$ BMDM in the CAM-activated state (P $<$ 0.01, Figure 1L). Glycerophosphorylcholine (GPC) was 0.81-fold lower in $Fatp1^{-/-}$ BMDMs in the unstimulated state (P $<$ 0.0001); however, upon CAM activation, $Fatp1^{-/-}$ BMDMs contained 1.20-fold (P $<$ 0.001) greater GPC compared to $Fatp1^{+/+}$ in respective states. Finally, eicosanoids were detected in media from the same BMDM experiment where metabolites in lysates were measured (Table A3). One of the most strikingly regulated eicosanoids was 15-Hydroxyicosatetraenoic acid (15-HETE), which was significantly upregulated in unstimulated and CAM activated $Fatp1^{-/-}$ compared to $Fatp1^{+/+}$ BMDM (P $<$ 0.0001 for both states, Figure 1M and Table A3). Other arachidonic acid metabolites including 12-HETE and 5-HETE as well as linoleic acid metabolite 9,10-Dihydroxy-12Z-octadecenoate (9,10-di-HOME) were also significantly increased in $Fatp1^{-/-}$ compared to $Fatp1^{+/+}$ BMDM (P $<$ 0.05, Table A3).

3.4. A lack of MΦ FATP1 exacerbated HFD-induced weight gain and induced glucose intolerance and greater accretion of epididymal white adipose tissue (eWAT)

Because *Fatp1* regulated substrate metabolism and directed MΦ activation *in vitro*, we sought to test effects of loss of function *in vivo*. We first demonstrated that *Fatp1* mRNA was elevated 7.5-fold in F4/80 + ATMs isolated from the stromovascular fraction from obese eWAT compared to lean mice at 23 weeks of age (Figure A5 A, P $<$ 0.001). Based on the fact that *Fatp1* is expressed in obese ATMs and may play a role in MΦ lipid metabolism and inflammation, we next created chimeras to study *Fatp1* deficiency in ATM function. Male C57BL/6J recipient mice were randomized onto either LFD or HFD at 3 weeks of age so mice would remain lean or gain weight, respectively. After 3 weeks on the diets (i.e., at 6 weeks of age), fasting glucose and MRI-determined body composition were identical for all mice regardless of diet group (data not shown). At this time point, recipient mice

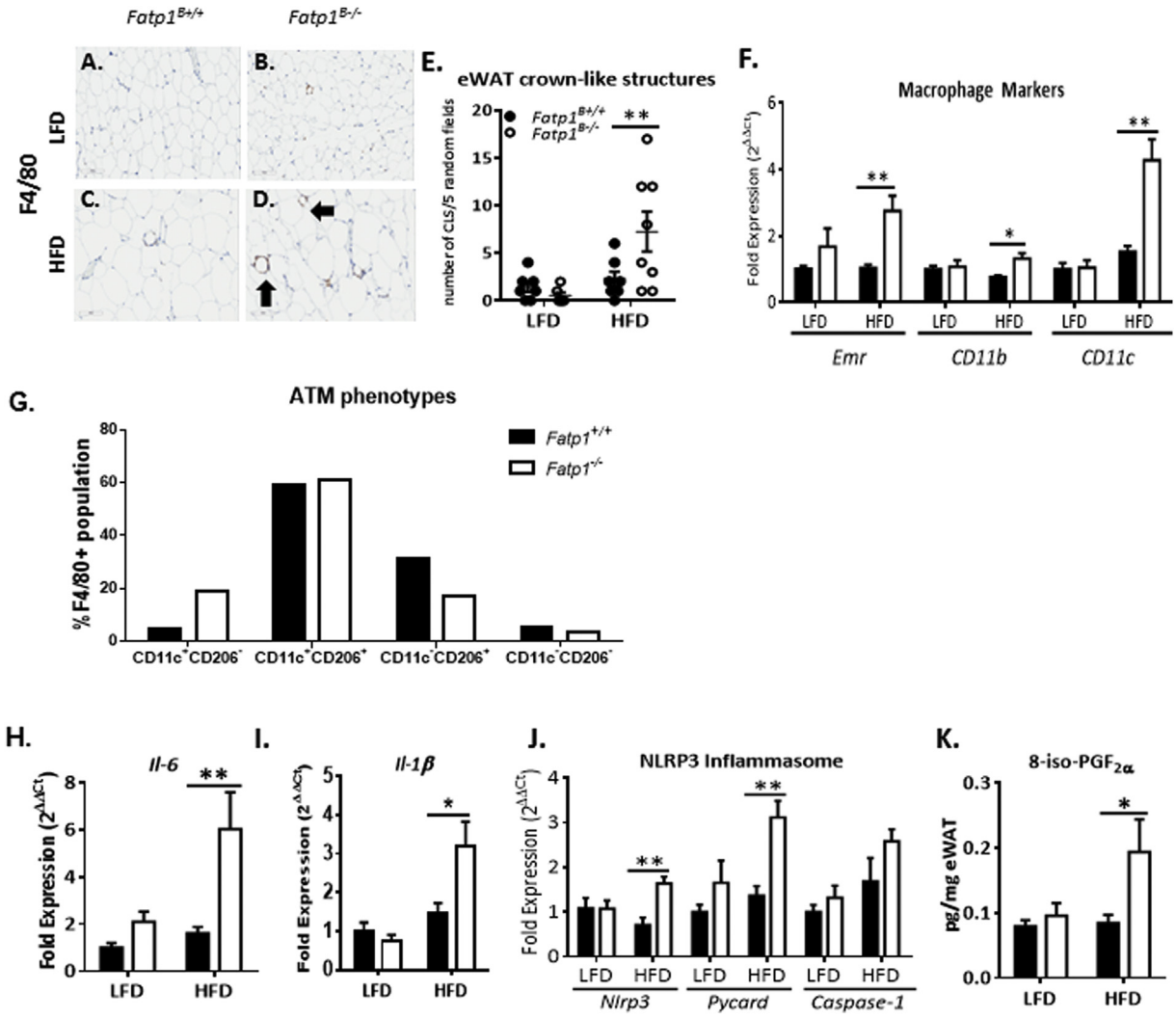

Figure 3: Lack of MΦ FATP1 increased adipose inflammation, shifted ATM phenotype, increased inflammasome expression and oxidative stress in HFD-fed mice. A–D. F4/80+ MΦ staining was conducted in eWAT. Representative 10X images are presented. E. Quantification of crown like structures (CLS, arrows in D) in eWAT in 5 random 20X fields ($P < 0.01$ in $Fatp1^{B+/+}$ vs. $Fatp1^{B-/-}$). F. mRNA expression of MΦ markers *Emr1* (*F4/80*), *Cd11b* and *Cd11c* was measured by qPCR in eWAT (**$P < 0.01$ and *$P < 0.05$ $Fatp1^{B+/+}$ vs. $Fatp1^{B-/-}$ within the same diet group). G. Flow cytometric analysis of % F4/80 + CD11c-eFluor450 and % F4/80 + CD206-APC positive staining in $Fatp1^{B+/+}$ and $Fatp1^{B-/-}$ ATMs cells isolated from eWAT stromovascular fraction from eWAT from $Fatp1^{B+/+}$ and $Fatp1^{B-/-}$ mice fed HFD for 23 weeks (N = 3). *Il-6* (H) and *Il-1β* (I) mRNA expression was measured by qPCR (**$P < 0.01$,*$P < 0.05$). J. Inflammasome mRNA expression in eWAT was measured by qPCR (**$P < 0.01$). K. Oxidative damage was assessed by 8-iso-$PGF_{2\alpha}$ concentration (*$P < 0.05$). Data shown are means ± SEM; differences detected by two-way ANOVA; N = 7–9 mice per group.

were lethally irradiated and transplanted with bone marrow from $Fatp1^{+/+}$ and $Fatp1^{-/-}$ donor mice to generate chimeric mice harboring either $Fatp1^{bonemarrow+/+}$ ($FATP1^{B+/+}$) or $Fatp1^{bonemarrow-/-}$ ($Fatp1^{B-/-}$) (see study design cartoon in Figure A5 B). Control mice that were irradiated but did not receive marrow died within 10 days of irradiation (data not shown). To confirm successful ablation and reconstitution of *Fatp1*-deficient marrow, BMDM were isolated from a cohort of LFD-fed and HFD-fed $Fatp1^{B+/+}$ and $Fatp1^{B-/-}$ mice. There were no significant differences in number or appearance of BMDM isolated from the transplanted and diet-exposed mice (data not shown). Figure A5 C illustrates that the irradiation and reconstitution with $Fatp1^{+/+}$ or $Fatp1^{-/-}$ marrow was successful as only the mutated *Fatp1* null allele, not wildtype *Fatp1*, was detectable in BMDM isolated from mice transplanted with $Fatp1^{-/-}$ bone marrow. Gene expression (not shown) and immunoblot analysis of these BMDM demonstrated that FATP1 was successfully ablated from MΦs in this model (Figure A5 D). In addition, hematologic and flow cytometric analysis of $Fatp1^{+/+}$ and $Fatp1^{-/-}$ mice demonstrated no significant differences in any measure including white blood cells, lymphocytes, granulocytes, monocytes, by either total numbers of cells or percentage of cells within the total blood cell population (Table A4 and A5). After irradiation and reconstitution, $Fatp1^{B-/-}$ mice gained significantly more weight compared to $Fatp1^{B+/+}$ on HFD ($P < 0.0001$ from 15 weeks through to sacrifice at 23 weeks on diet) (Figure 2A). After 23 weeks on diet, random-fed blood glucose concentrations were 14% higher in $Fatp1^{B-/-}$ mice compared to $Fatp1^{B+/+}$ on HFD ($P < 0.05$, Figure 2B). Six-hour-fasted blood glucose concentrations did not differ significantly by genotype; LFD-fed $Fatp1^{B+/+}$, and $Fatp1^{B-/-}$ fasted blood glucose concentrations at termination were an average of 133 mg/dL for both genotypes, whereas HFD-fed concentrations were 131.5 and 147 mg/dL, respectively. Six-hour-fasted plasma insulin concentrations at termination revealed no significant differences

among the groups (supplemental Figure A6 A). Likewise, there were no differences in homeostasis model assessment of insulin resistance ($HOMA_{IR}$) or homeostasis model % β cell function ($HOMA_{\%\beta}$) (data not shown).

Glucose tolerance tests (GTT) were performed to evaluate systemic metabolic responses in $Fatp1^{B+/+}$ and $Fatp1^{B-/-}$ LFD- and HFD-fed mice. Overall, HFD in this BMT model did not induce dramatic defects in glucose disposal, which was expected and similar to other BMT models due to lack of extensive weight gain associated with irradiation [42,57,58]. However, circulating glucose concentration at 15 min post glucose injection was significantly higher in $Fatp1^{B-/-}$ mice on HFD ($P < 0.001$), which correlated to delayed and inefficient disposal of glucose compared to $Fatp1^{B+/+}$ for the remainder of the time course (30 min: $P = 0.004$; 60 min: $P = 0.03$, 120 min: $P = 0.04$) (Figure 2C). Insulin tolerance tests (ITT) indicated that neither diet nor genotype affected the glucose response to an injection of insulin (supplemental Figure A6 B and C). Furthermore, histologic and immunohistologic analysis of insulin staining and morphology of islets in pancreata did not demonstrate significant alterations in number or size of islets between diet and genotypes (supplemental Figure A6 D). Finally, eWAT was analyzed in mice that received insulin prior to sacrifice to determine insulin signaling capacity (supplemental Figure A6 E). Quantification revealed that in LFD-fed mice, regardless of genotype, insulin induced a 1.5—2-fold increase in pAKT/AKT concentrations. There was no Fatp1 genotype effect; however, insulin-stimulation reached significance in $Fatp1B^{+/+}$ ($P = 0.041$) but failed to reach significance in $Fatp1B^{-/-}$ LFD-fed mice. In mice fed HFD, the insulin response was only 1-fold as compared to 1.5—2-fold in lean mice. The insulin response was statistically reduced in HFD-fed mice compared to LFD-mice in both $Fatp1B^{+/+}$ ($P = 0.0008$) and $Fatp1B^{-/-}$ ($P = 0.0008$).

Body composition was next investigated to determine if MΦ FATP1 contributed to alterations in adipose tissue. Mice fed a HFD displayed significantly increased percent body fat as measured by MRI as well as elevated plasma leptin concentrations ($P < 0.001$, Figure A7 A and B, respectively). A trend for $Fatp1^{B-/-}$ mice to have greater adiposity and leptin was evident, yet no significant genotype differences were detected. However, isolated eWAT depots in HFD-fed $Fatp1^{B-/-}$ mice were 40% heavier compared to HFD-fed $Fatp1^{B+/+}$ mice ($P < 0.01$, Figure 3 D). Neither lean mass nor liver and brown adipose weights were altered by genotype (Figure A7 C—E). Furthermore, no difference was found in respiratory exchange rate (RER), measured by metabolic chamber, during the day or at night between $Fatp1^{B-/-}$ and $Fatp1^{B+/+}$ mice either on LFD or HFD despite a significant nighttime diet effect ($P = 0.01$) (Figure A7 F and G).

3.5. Deletion of MΦ *Fatp1* led to augmented eWAT MΦ influx, crown-like structure (CLS) formation, inflammation, activation of the NLRP3 inflammasome, and oxidative damage in HFD-fed mice

Infiltration of MΦs from transplanted marrow into eWAT was confirmed by PCR-based genotyping of eWAT genomic DNA to detect the mutated *Fatp1* allele (Figure A7 H). There was a 60% increase in the number of F4/80 + CLS observed in eWAT from HFD-fed $Fatp1^{B-/-}$ mice compared to HFD-fed wild type controls (Figure 3A—D and quantified in 3E, $P < 0.01$). Furthermore, qPCR gene expression analysis for monocyte/MΦ markers *Emr1* (F4/80), *Cd11b*, and *Cd11c* indicated significant increases in HFD-associated MΦ influx in HFD-fed $Fatp1^{B-/-}$ eWAT compared to $Fatp1^{B+/+}$ (2.7-fold higher, $P < 0.01$; 1.7 fold, $P < 0.05$; and 2.8-fold, $P < 0.001$, respectively, Figure 3F). Importantly, flow cytometric analysis of F4/80 + macrophages from the SVF of eWAT demonstrated that more CAM-like CD11c + CD206- ATMS were present in eWAT from $Fatp1^{B-/-}$ mice compared to $Fatp1^{B+/+}$ on HFD. Likewise, a decrease in AAM-like CD11c-CD206+ ATMS were present in eWAT from $Fatp1^{B-/-}$ mice compared to $Fatp1^{B+/+}$ on HFD (Figure 3G, with gating strategy and scatter plots in Figure A8 A and B respectively).

Upon the discovery of greater MΦ influx and a shift towards more inflammatory ATM phenotype in $Fatp1^{B-/-}$ mice compared to $Fatp1^{B+/+}$ on HFD, we next investigated pro-inflammatory cytokine expression. Expression of the pro-inflammatory cytokine *Il-6* was 5-fold higher in eWAT from $Fatp1^{B-/-}$ mice compared to $Fatp1^{B+/+}$ on HFD ($P < 0.01$, Figure 3H). Likewise, expression of the pro-inflammatory cytokine *Il-1β*, was doubled in eWAT from $Fatp1^{B-/-}$ mice compared to $Fatp1^{B+/+}$ on HFD ($P < 0.05$, Figure 3I). IL-1β production results from activation of the inflammasome [59]. We observed significantly elevated expression of NLRP3 inflammasome subunits including *Nlrp3* and *Pycard* in eWAT from $Fatp1^{B-/-}$ mice compared to $Fatp1^{B+/+}$ on HFD ($P < 0.01$, Figure 3J). Furthermore, elevated 4-HNE (data not shown) and significantly increased concentrations of 8-iso-$PGF_{2\alpha}$, an indicator of non-enzymatic oxidative damage, indicated increased oxidative damage in eWAT from HFD-fed $Fatp1^{B-/-}$ mice compared to HFD-fed $Fatp1^{B+/+}$ mice ($P < 0.05$, Figure 3K). Finally, there were trends for increased eicosanoids in LFD-fed eWAT such as 15-HETE, 5-HETE and 9,10-DiHOME (metabolites that were significantly regulated in BMDMs by *Fatp1*), however these did not reach statistical significance in eWAT (data not shown).

3.6. FATP1 gain of function model drove ACSL activity and fatty acid uptake

Given that lack of Fatp1 led to dramatic changes *in vitro* and *in vivo*, we next determined if the highly glycolytic CAM-like RAW264.7 mouse MΦ cell line could be metabolically reprogrammed toward an AAM-like phenotype via FATP1 overexpression (FATP1-OE). First, expression levels of the 6 members of the *Fatp* family were examined by qPCR. RAW MΦs expressed only *Fatp1* and *Fatp4*, both of which were induced 2-fold by 24 h LPS activation (Figure 4A). *Fatp2*, 3, 5, and 6 were not detected. Overexpression of both *Fatp1* mRNA ($P < 0.001$, Figure 4A) FATP1 protein in FATP1-OE was achieved compared to empty vector controls (FATP1-EV, Figure 4B). FATP1 protein is essentially undetected in unstimulated RAW MΦs, thus FATP1 overexpression created a gain of function model. A significant decrease in *Fatp4* expression in FATP1-OE MΦs upon LPS activation was evident compared to FATP1-EV ($P < 0.05$). FATP1 over expression had no effect on cell size, viability, or growth (Figure A2 D—E).

ACSL activity assays were performed on FATP1-EV and FATP1-OE MΦs to ensure that the over-expressed FATP1 was functional. Total ACSL activity was increased by 20% in FATP1-OE compared to FATP1-EV ($P < 0.05$, Figure 4C). A 17% increase in fatty acid uptake was detected in FATP1-OE compared to FATP1-EV in the unstimulated state ($P < 0.01$, Figure 4D). LPS activation increased fatty acid uptake by 2.3-fold in FATP1-EV, while FATP1-OE showed a 2.7-fold increase. Thus, fatty acid uptake in FATP1-OE was 36% greater than FATP1-EV in LPS-stimulated cells ($P < 0.0001$, Figure 4D).

3.7. FATP1 overexpression reprograms RAW MΦs toward an AAM-like metabolic phenotype.

We next evaluated the capacity for metabolic flexibility in the RAW MΦ cell line. There were no FATP1-mediated differences in either complete or incomplete oleate oxidation (Figure A2 F and data not shown). LPS-activation of RAW MΦ led to dramatically reduced complete fatty acid oxidation regardless of FATP1 genotype, demonstrating a disconnect between fatty acid uptake and oxidation (Figure 4D and A2 F). At

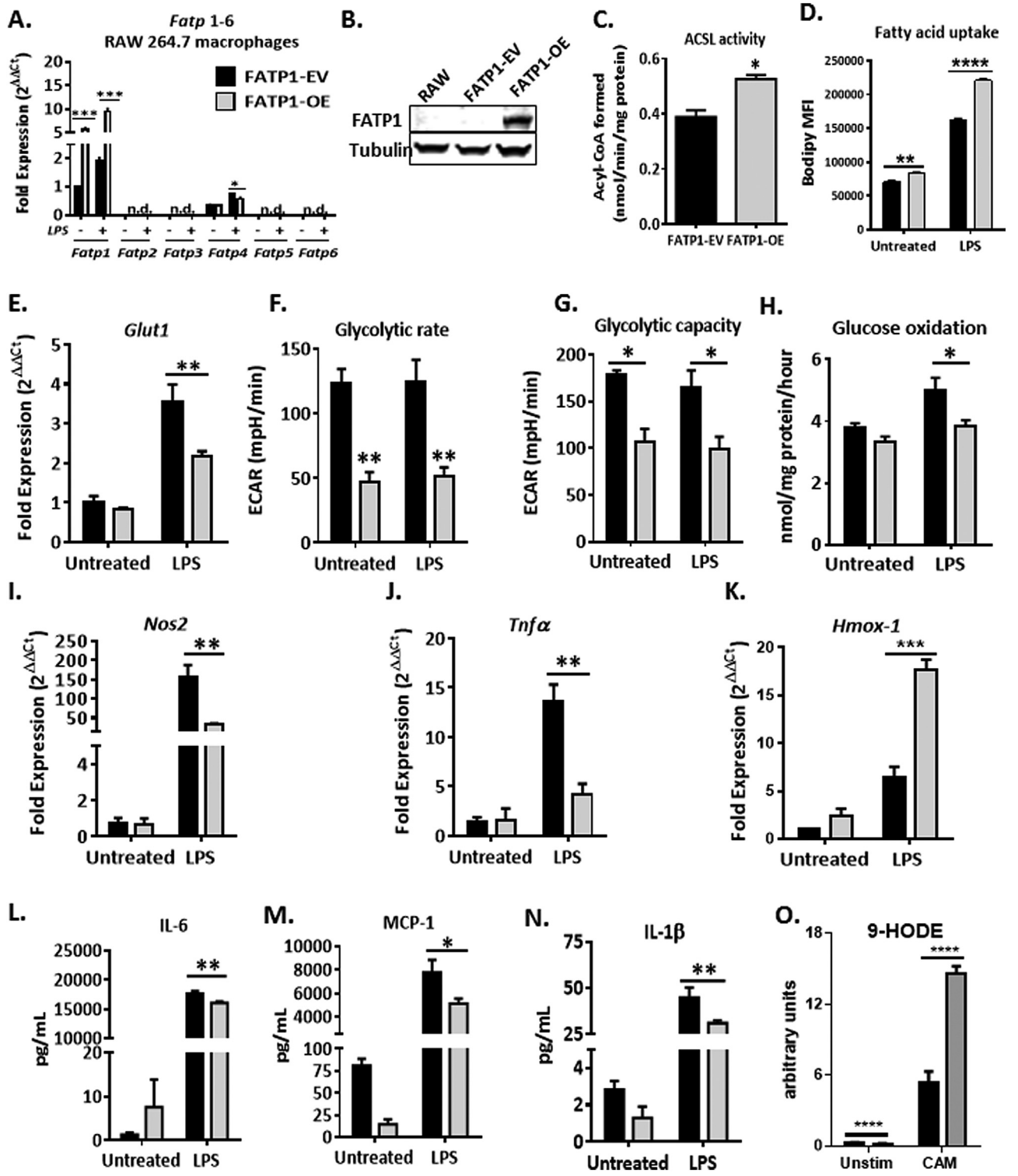

Figure 4: Overexpression of FATP1 in RAW264.7 MΦs induced a substrate switch with enhanced lipid metabolism and reduced glucose metabolism resulting in blunted CAM-activation. *Fatp1* was stably over-expressed in RAW264.7 MΦs (FATP1-OE) and controls were empty vector (FATP1-EV). A. *Fatp1-6* were measured by qPCR (n.d., not detected; ***P $<$ 0.001, *P $<$ 0.05). B. FATP1 Western immunoblot in unstimulated RAW264.7 (RAW) MΦs, FATP1-EV, and FATP1-OE. Tubulin was used as a loading control. C. FATP1-mediated long chain ACSL activity was measured using ^{14}C—oleate (*P $<$ 0.05). FATP1-EV and FATP1-OE were left untreated or stimulated for 24 h with 100 ng/ml LPS. D. Fatty acid uptake was measured using BODIPY®-palmitate (**P $<$ 0.01, ***P $<$ 0.001). E. *Glut1* expression was measured by qPCR (**P $<$ 0.01). Glycolytic rate (F) and glycolytic capacity (G) were measured using a Seahorse Bioanalyzer (**P $<$ 0.01, *P $<$ 0.05). ^{14}C-glucose oxidation (H) was measured (*P $<$ 0.05). Data are mean ± SEM. Representative of at least N = 3 experiments with n = 4 replicates per experiment. mRNA expression was measured by qPCR for *Nos2* (I) and *Tnfα* (J) and *Hmox-1* (K) (**P $<$ 0.01, ***P $<$ 0.001). Secreted IL-6 (L) and MCP-1 (M) and IL-1β (N) were measured by Luminex (**P $<$ 0.01, *P $<$ 0.05). Data are mean ± SEM; differences were detected by two-way ANOVA. Representative of at least N = 3 experiments with n = 4 replicates per experiment. O. Metabolite 9-HODE was measured in BMDM lysates (****P $<$ 0.0001 for both unstim and CAM FATP1-EV vs. FATP1-OE, N = 4).

baseline, there were no significant differences in *Glut1* expression, however with LPS stimulation *Glut1* expression was 39% lower in FATP1-OE compared to FATP1-EV ($P < 0.01$, Figure 4E). Acute glucose uptake was reduced in FATP1-OE MΦs, though this result did not reach statistical significance (Figure A2 G). However, long-term bioenergetics measurements demonstrated a significant 60% reduction in glycolytic rate in FATP1-OE MΦs compared to FATP1-EV controls in both unstimulated and LPS-stimulated conditions ($P < 0.01$, Figure 4F). Glycolytic capacity was also significantly reduced with FATP1 overexpression to levels 60% of those in FATP1-EV ($P < 0.05$, Figure 4G). In addition, FATP1-OE MΦs demonstrated a 23% reduction in glucose oxidation upon LPS-activation ($P < 0.05$, Figure 4H). Finally, glycogen synthesis was unaffected by FATP1 expression in either unstimulated or LPS-activated MΦs (data not shown).

3.8. FATP1 gain of function inhibited MΦ pro-inflammatory response

To examine the consequence of FATP1-mediated alterations in metabolism on the inflammatory response in RAW MΦ, pro- and anti-inflammatory mediators in unstimulated and LPS-stimulated cells were examined. In direct contrast to expression patterns observed in *Fatp1*$^{-/-}$ BMDM, FATP1 overexpression significantly suppressed the induction of LPS-induced pro-inflammatory enzyme *Nos2* ($P < 0.01$, Figure 4I) and cytokine *Tnf-α* ($P < 0.01$, Figure 4J). *Hmox-1* expression was 2.3- and 2.8-fold higher in unstimulated and activated FATP1-OE, respectively (Figure 4K). Secretion of IL-6 and MCP-1 protein was significantly diminished in response to LPS stimulation in FATP1-OE compared to FATP1-EV ($P < 0.01$ and $P < 0.05$, Figure 4L and M, respectively). IL-1β protein secretion was also significantly reduced in FATP1-OE compared to FATP1-EV ($P < 0.01$, Figure 4N). AAM-markers *Mrc-1* and *Arginase-1* were not detectable in FATP1-EV and FATP1-OE cells in either the unstimulated or LPS-stimulated state.

3.9. Metabolomic and lipidomic analysis demonstrated that FATP1 overexpression down-regulated glucose metabolic pathways and biomarkers of oxidative stress

Based on significant alterations to metabolism and inflammation, we next used metabolomics and lipidomics to query potential mediators or biomarkers associated with *Fatp1*. Metabolomic profiling revealed that RAW264.7 MΦs are highly metabolically active, especially in comparison with BMDM, because they are proliferating as an immortalized cell line (Tables A1 and A2). In total, CAM activated upregulated 116 or 97 metabolites, with 25 or 56 downregulated in FATP1-EV or FATP1-OE, respectively. In contrast to BMDM, RAW MΦs that were CAM stimulated greatly upregulated amino acid metabolism, did not downregulate dipeptides, and greatly increased metabolites in carbohydrate metabolism and the Krebs cycle. CAM activated RAW MΦs also upregulated lipid metabolism including many fatty acid metabolites, glycerolipids, and sphingolipids (but downregulated lysolipids). RAW activation also increased pyridoxal metabolism, riboflavin metabolism and thiamine metabolism, while BMDM did not regulate these metabolites.

CAM stimulation of the RAW model altered the biochemical profiles of FATP1-EV and FATP-OE along parallel but distinct trajectories (supplemental Figure A4). Upon examining effects of FATP1 gain of function on metabolites, FATP1 overexpression resulted in an up-regulation of 40 and down-regulation of 73 metabolites in unstimulated RAW cells, while CAM activation resulted in up-regulation of 38 and downregulation of 120 metabolites in FATP1-OE compared to FATP1-EV (Table A2, and P values within). Regardless of activation state (unstimulated or CAM activated), examples of metabolites significantly *downregulate*d by FATP1-OE included glutamate and glutamine, reduced glutathione (GSH), glucose, 3-phosphoglycerate, PRPP, UDP-glucose, citrate, butyrlcarnitine, choline phosphate, palmitoyl sphingomyelin and stearoyl sphinomelin, inosine, and AMP (Table A2, and P values within, a subset are highlighted in pathway in supplemental Figure A9 A). Examples of metabolites significantly *upregulated* by FATP1-OE (regardless of activation state) include pyroglutamine, gamma-aminobutyrate (GABA), imidazole propionate, 3-(4-hydroxyphenyl)lactate, 5 aminovalerate, 4-guaninobutanoate, sorbitol, ribitol, 2-hydroxyglutarate, deoxycarnitine, 2-dehydrocarnitine, acetylcarnitine, ethanolamine, choline, 5-methyltetrahydrofolate, and riboflavin vitamin B2 (Table A2, and P values within, and pathway supplemental Figure A9 A). Furthermore, regardless of activation, several fatty acids were downregulated, including essential fatty acids (docosapentaenoate (n3 DPA; 22:5n3), docosapentaenoate (n6 DPA; 22:5n6), docosahexaenoate (DHA; 22:6n3)), stearate (18:0), arachidonate (20:4n6), and adrenate (C22:4n6), reaching significance in CAM-stimulation for all fatty acids listed, with the exception of adrenate, which reached significance in both unstimulated and stimulated states. Of note, arachidonate (20:4n6) was essentially undetectable in FATP1-OE after CAM stimulation. Interestingly, not every long chain fatty acid was downregulated; eicosenoate (20:1n9 or 11) and docosatrienoate (22:3n3) were upregulated. Finally, intracellular lipid metabolite 9-hydroxy-10,12-octadecadienoic acid (9-HODE) was essentially undetectable in unstimulated cells but was significantly 3-fold increased in activated FATP1-OE CAM stimulated cells ($P = 0.0001$ for FATP1-EV vs. FATP1-OE, Figure 4O).

When cells were CAM activated compared to unstimulated, FATP1-EV controls upregulated metabolites in the Krebs cycle including citrate, succinate, fumarate, and malate, while FATP1-OE downregulated these metabolites (Table A2, supplemental Figure A9 A). In contrast, many lysolipids were upregulated with CAM stimulation in FATP1-OE that were not regulated or downregulated in control EV cells, including 1-palmitoylglycerophosphocholine, and 1-stearoylglycerophosphocholine. In line with radiotracer and bioenergetic data, FATP1-OE demonstrated significant down-regulation of glucose in both unstimulated and CAM-activated cells. PPP metabolites including phosphoribosyl pyrophosphate (PRPP), 6-phosphogluconate, xanthine, inosine, and UDP-glucuronate were at lower concentrations in CAM-activated FATP1-OE compared to CAM-activated FATP1-EV controls (Table A2, supplemental Figure A9 A).

One-carbon metabolism was also significantly altered with FATP1 overexpression in CAM. Concentrations of choline, betaine, glycerophosphocholine and S-adenosylmethionine (SAM) were significantly increased in CAM stimulated cells while metabolites downstream of SAM were decreased, specifically methionine and cysteine in FATP1-OE compared to FATP1-EV controls. Differences in B-vitamins were observed with decreased pantothenate (B_5) and increased riboflavin (vitamin B_2) in CAM stimulated cells with FATP1 overexpression. Furthermore, a significant, greater than 2-fold, decrease in citrulline concentration and a concomitant increase in polyamine spermidine and polyamine-associated metabolite 5-methylthioadenosine (5-MTA) in FATP1-OE upon CAM stimulation was detected (Table A2, and P values within, pathway in supplemental Figure A9 B) [60]. Epigenetic modification of macrophages is important [61,62]; FATP1 regulates important methyl donors such as SAM (supplemental Figure A9 B). Finally, significant reductions in markers of oxidative stress were detected in FATP1-OE CAM activated cells compared to FATP1-EV including methionine sulfoxide, cysteineglutathione disulfide, and 2-

aminoadipate (supplemental Figure A10 A–C, P = 0.01, 0.0001, and 0.0001, respectively).

3.10. FATP1 overexpression reduced free arachidonic acid and certain eicosanoid synthesis

Because FATP1 is a long and very long chain ACS, we next investigated long chain fatty acids including arachidonic and lineolate acid and eicosanoid metabolism in our RAW control and gain of function model. Significant alterations in arachidonate (20:4n6) were evident in FATP1-OE lysates using metabolomic analysis with an 85% reduction when FATP1 was over expressed ($P < 0.05$ FATP1-EV vs. FATP1-OE, Figure 5A). Hence, we investigated eicosanoid metabolism in our RAW control and gain of function model. Arachidonate metabolites including 15-HETE, 12-HETE and 5-HETE were significantly downregulated in the media by overexpression of FATP1 ($P < 0.0001$ in both unstimulated and CAM activated cells, Figure 5B–D). Linoleate (18:2n6) was significantly upregulated by 50% in FATP1-OE in unstimulated cell lysates ($P < 0.05$, Table A2) and non-significantly downregulated by 20% in CAM activated cells. When media was examined from the same cells, FATP1-OE significantly downregulated linoleate metabolite 9,10-diHOME ($P < 0.0001$, Figure 5E and Table A3).

3.11. *FATP1* variants are associated with *FATP1* expression levels in human adipose

We searched public databases for genetic variants located within 1 Mb of *FATP1* that were associated with *FATP1* expression (eQTLs) in

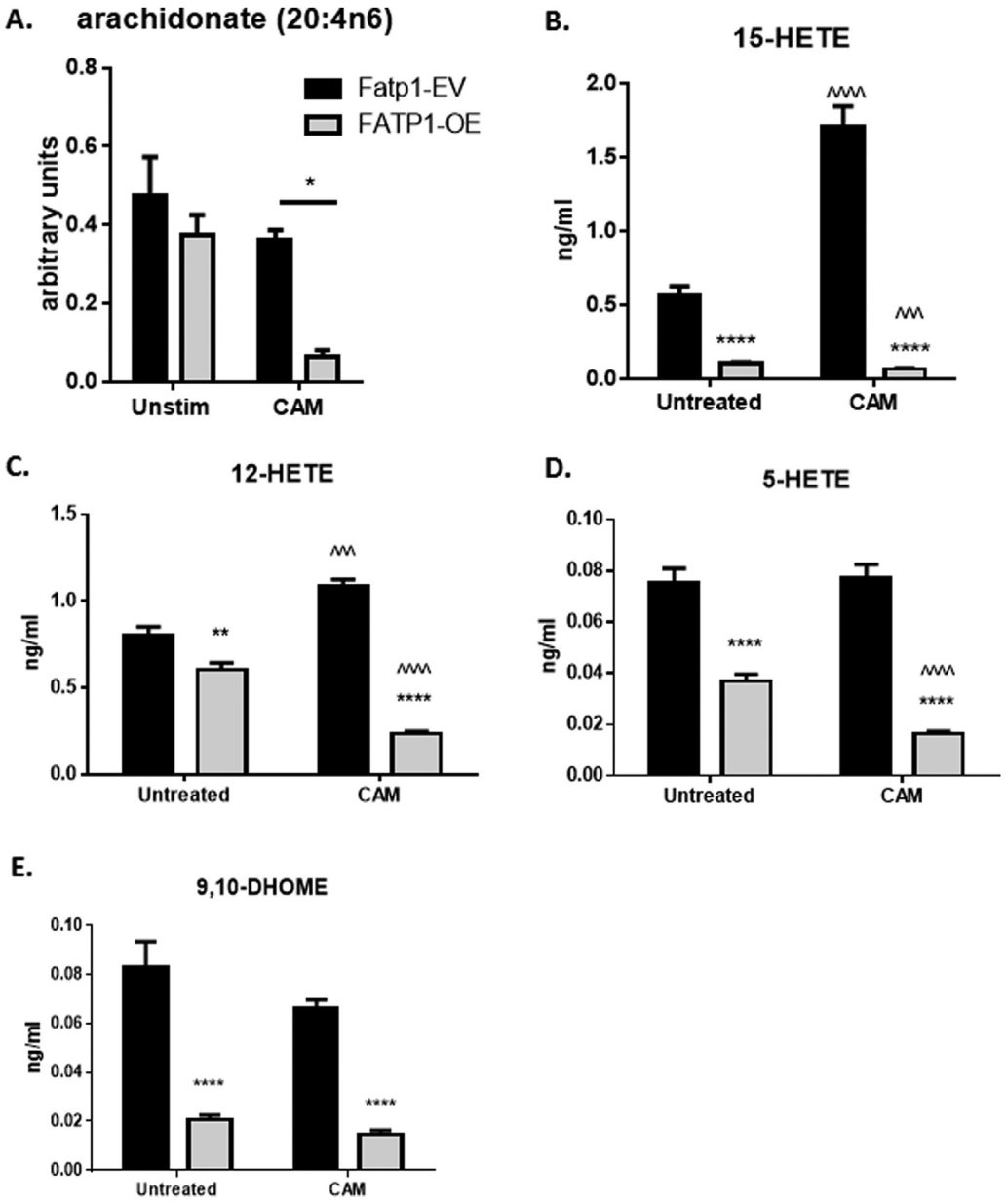

Figure 5: Overexpression of FATP1 in RAW264.7 MΦs decreased arachidonate and certain eicosanoid concentrations. A. Arachidonate (20:4n6) was measured in cell lysates using metabolomics analysis (*$P < 0.05$ FATP1-EV vs. FATP1-OE) B–E. Eicosanoids were measured in conditioned cell media. 15-HETE, 12-HETE and 5-HETE (**$P < 0.01$, ****$P < 0.0001$ FATP1-EV vs. FATP1-OE; Ƥ < 0.001 and Ƥ < 0.0001 unstimulated vs. CAM). F. Linoleate metabolite 9,10-diHOME was measured in conditioned cell media (****$P < 0.0001$).

human adipose tissue. The Multiple Tissue Human Expression Resource (MuTHER) study of 856 female twins showed the strongest eQTL for *FATP1* with rs9137 ($P = 1.3 \times 10^{-13}$), which is located in the 3′UTR of *FATP1*. In the METabolic Syndromes In Men (METSIM) study of 1,381 men, the strongest association with adipose *FATP1* expression was observed for rs3212793 ($P = 1.8 \times 10^{-4}$), located ~300 kb downstream of the *FATP1* gene. These results demonstrate that *FATP1* levels vary between individuals and that these and/or other nearby variants may be involved in the regulation of *FATP1* expression.

4. DISCUSSION

Over the past 35 years, the prevalence of obesity has increased in both Western nations and globally [63]. Immune-based therapies offer promising interventions for obesity induced Type 2 Diabetes [64,65] including several approaches aimed at increasing insulin sensitivity by blocking the action of inflammatory mediators. Specifically, previous reports implicate IL-1α, IL-1β, TNFα, MCP-1 (CCL2), and IL-6 [64–70]. Our previous work demonstrated that modulating bioactive lipid generation and trafficking in MΦs is an effective tool against obesity, insulin resistance, and diabetes [71–73]. Thus, we hypothesized that maintaining sufficient lipid metabolism by modulating transport and metabolism of specific fatty acids would suppress ATM-mediated inflammation and preserve metabolic health. FATP1 is a fatty transporter through its capacity to trap long and very long chain fatty acids intracellularly via its ACSL activity. ACSL-mediated generation of acyl-CoAs targets fatty acids to certain metabolic fates, which may participate in the regulation of inflammation. Herein, to study FATP1 in MΦ biology, complementary *ex vivo* BMDM loss-of-function and *in vitro* RAW MΦ gain-of-function models as well as LFD- and HFD-exposed mice were used to elucidate the metabolic and mechanistic alterations stemming from modulation of *Fatp1* expression.

BMDM and RAW MΦs express only *Fatp1* and *Fatp4*. No compensatory expression of other *Fatp* gene family members was detected in response to loss of FATP1. Therefore, total ACSL activity was significantly reduced in $Fatp1^{-/-}$ BMDM, demonstrating that while other ACSLs are present to activate fatty acids, such as ACSL1 [74], there was a lack of enzymatic compensation overall. Metabolic and bioenergetics analysis of $Fatp1^{-/-}$ BMDM demonstrated that along with reduced ACSL activity, deletion of *Fatp1* resulted in blunted fatty acid uptake and oxidation, particularly in AAM-activated BMDMs, which are established to be more fatty acid-dependent. Findings of reduced fatty acid uptake and oxidation occurred even in the setting of elevated oxygen consumption rate in $Fatp1^{-/-}$ compared to $Fatp1^{+/+}$ BMDMs, suggesting that there was no global defect in mitochondrial capacity. In fact, anapleurotic substrates and BCAA were decreased in CAM-activated $Fatp1^{-/-}$ BMDM, which could have driven and sustained the observed elevated mitochondrial respiration. Importantly, deletion of *Fatp1* reprogrammed MΦs: a shift in metabolism toward increased carbohydrate metabolism was detected. Notably, increased *Glut1*, glycolysis and PPP metabolites were evident. Furthermore, both glycolytic rate and capacity were inversely proportional to ACSL activity. Less lactate was detected in $Fatp1^{-/-}$ BMDMs, corroborating the increase in extracellular lactate as measured by ECAR. Taken together, greater OCR, ECAR, and glycolytic metabolites indicated that $Fatp1^{-/-}$ MΦs have a higher energetic status compared to $Fatp1^{+/+}$ MΦs [75]. Deletion of *Fatp1* fundamentally altered an aspect of mitochondrial, biogenesis, function or activity of the electron transport chain, perhaps uncoupling, which is under further investigation. Spearman correlation analyses revealed a significant inverse correlation between glycolytic rate and fatty acid oxidation, demonstrating the compensatory responsiveness of these pathways, or metabolic flexibility, in response to lack of *Fatp1*. The shift from fatty acid oxidation to increased glycolysis appears to create a more CAM-like phenotype of MΦ lacking *Fatp1*. Indeed, lack of *Fatp1* resulted in increased *Nos2* expression, a hallmark of CAM activation, as well as reduced *Arginase-1* expression, a classic AAM marker, and *heme oxygenase 1*, an anti-inflammatory enzyme. CAM induction of iNOS and NO production leads to NO-mediated downregulation of the electron transport chain, providing a direct link between inflammation and metabolism [23]. In sum, data suggest that while the lack of Fatp1 appears to activate mitochondrial activity, specific defects in fatty acid uptake and oxidation are linked to the inflammatory phenotype in the MΦ.

Since *ex vivo* BMDM studies were supportive of FATP1 reducing pro-inflammatory activation of MΦ, the role of FATP1 in diet-induced metabolic dysfunction was investigated next. Using a model of HFD-induced weight gain, we investigated the contribution of MΦ FATP1 to inflammation and glucose tolerance. ATMs isolated from obese adipose expressed greater *Fatp1* than ATMs from lean mice, demonstrating the relevance of this transporter to obesity-associated MΦ function and lipid trafficking. Importantly, ATMs isolated from mice fed HFD demonstrated that, in the absence of *Fatp1*, ATMs were polarized towards CAM phenotype and less towards AAM. Thus, we provide evidence that $Fatp1^{B-/-}$ ATMs fail to maintain the AAM phenotype and are skewed towards CAM compared to $Fatp1^{B+/+}$ ATMs, akin to *in vitro* loss of function BMDM studies. A detailed time course would be ideal to understand *Fatp*1's regulation on AAM and CAM ATMs during obesogenesis.

In striking contrast to the total-body $Fatp1^{-/-}$ mice [29,30], we report that chimeric mice harboring MΦ that were deficient in *Fatp1* were more susceptible to diet-induced metabolic dysfunction including greater weight gain and adiposity, hyperglycemia, and glucose intolerance compared to diet-matched $Fatp1^{B+/+}$ mice. Impaired glucose tolerance occurred in the setting of no *Fatp1*-mediated differences in ITT, islet morphology, insulin signaling capacity, plasma insulin levels, or calculated HOMA scores. It is possible that the discrepancy between impaired glucose tolerance with no detectable impairment of ITT was due to the timing of the GTT at 19 weeks, while the ITT and plasma measures that occurred at sacrifice did not occur until 20 and 23 weeks on diet, respectively, when *Fatp1*-mediated effects may have been lost. In the LFD-fed lean state, no significant *Fatp1*-mediated effects were observed, demonstrating that HFD-induced stress was necessary to observe the phenotype. Importantly, there were no significant differences in circulating immune cell population numbers by hematologic and flow cytometric analysis in cells isolated from whole body $Fatp1^{-/-}$ mice compared to $Fatp1^{+/+}$, demonstrating that FATP1 does not likely play a strong role in hematopoiesis. There were also no differences in metabolic activity such as RER in LFD- or HFD-fed mice in a *Fatp1*-dependent manner. Taken together, diet findings indicate that MΦ FATP1 plays a specific role in limiting HFD-induced metabolic dysfunction through local tissue homeostasis when deficiency is restricted to MΦs. The role of ACS activity in MΦ has been reported in only one other model. Deletion of ACSL1 *protected against* the CAM phenotype in diabetes and atherosclerosis [74]. Importantly, our directly opposed findings in our chimeric model highlight the existence of non-redundant roles for ACSLs within MΦs.

A primary limitation to the project was that the chimera was created by bone marrow transplantation, which inherently reduces the adipogenic capacity of HFD exposure [42,57,58]. Therefore, while significant effects were detected in the absence of *Fatp1* on HFD, the overall effect of HFD on components of metabolic syndrome compared to LFD-fed mice was limited. We acknowledge that our chosen study design of

irradiation and diet exposure did not lead to a greater weight gain differential between LFD- and HFD-fed wildtype-transplanted mice. Still, wildtype-transplanted HFD-fed mice developed larger fat pads by weight, greater fat mass by MRI, higher leptin, and had reduced RER, as well as blunted insulin signaling by Western immunoblot. Perhaps if a different diet, such as a sucrose-free LFD, a higher percent fat HFD, or a different diet exposure time course were chosen, then there would have been greater differences in weight gain and exaggerated FATP1-mediated metabolic dysfunction. Our results beg the question of MΦ-specific FATP1 effects, especially in an inducible manner. Thus, future directions include studying FATP1-mediated effects specifically on ATMs. Although *in silico* analysis using the ImmGen Project suggested that FATP1 is only detected on MΦs and plasmacytoid dendritic cells [35], it is possible that T, B or other granulocytes could express *Fatp1* at high levels in an obesity-dependent manner, which further supports the need for additional studies using MΦ-specific *Fatp1* over-expression and deletion.

MΦ FATP1 may affect adipogenesis and systemic glucose metabolism in several ways. First, $Fatp1^{B-/-}$ mice fed a HFD accumulated excess white adipose mass that was characterized by excessive CLS formation, MΦ infiltration, and inflammatory cytokine production. CLS are classic histologic markers of adipose inflammation and obesity associated with the metabolic syndrome [4]. Xu et al. have argued that adipose tissue inflammation is influenced to a greater extent by sheer MΦ number rather the phenotype of those MΦs [11]. Herein, we report an approximately 2-fold increase in MΦ marker expression, a 3-fold increase of CLS, and an overall shift toward a CAM phenotype in the absence of *Fatp1* (represented by a doubling of *Il-1β* and 3.7-fold higher *Il-6* expression) in HFD-$Fatp1^{B-/-}$ adipose tissue suggesting that both MΦ number and ATM phenotype were affected by FATP1 expression. In addition, data support that FATP1 plays a role in limiting both priming and activation of the NLRP3 inflammasome, which is an established regulator of inflammation. Obesity activates the NLRP3 inflammasome, a nutrient sensor and potent regulator of the innate immune system, leading to insulin resistance and diabetes [76]. The NLRP3 inflammasome is activated by a "two-hit" process initiated by many metabolites and other stimuli, thereby inducing CASPASE 1-mediated cleavage of pro-IL-1β to active IL-1β [76]. Once secreted, IL-1β induces production of cytokines and chemokines including IL-6, IL-8, TNFα, and monocyte chemoattractant protein 1 (MCP-1, or CCL2), which collectively promote further MΦ activation and migration [70]. Transcription of the NLRP3 inflammasome components and its product *Il-1β* was significantly increased in adipose from HFD-fed $Fatp1^{B-/-}$ compared to controls.

Oxidative stress is another hallmark of obesity. ROS are signaling cascade second messengers known to enhance expression of pro-inflammatory mediators. We and others have shown that persistent activation of ROS—generating pathways results in increased oxidative damage [20,77,78]. Using targeted metabolomics and immunohistochemistry, we detected increased adipose oxidative damage in HFD-fed $Fatp1^{B-/-}$ mice with reductions in small molecule biomarkers of oxidative stress including methionine sulfoxide, cysteineglutathione disulfide, and 2-aminoadipate in FATP1-OE. Methionine sulfoxide is a product of methionine oxidation and is a biomarker of oxidative stress [79]. Aminoadipic acid (2-aminoadipate) is a lysine breakdown metabolite that is a biomarker of oxidative stress and predicts diabetes risk [80—83]. Cysteineglutathione disulfide is a derivative of glutathione and can generate S-glutathionylation, a signaling molecule for oxidative stress [84]. Furthermore, it is possible that the high iNOS expression in the absence of *Fatp1* reported herein in BMDMs will also be found in ATMs and would explain the significant increase in oxidative damage detected in HFD-fed $Fatp1^{B-/-}$ adipose, which will be investigated future studies.

Comprehensive metabolic analysis of FATP1's effect on MΦ biology was undertaken to gain insight into pathways that may lead to elevated inflammation and/or oxidative stress. Metabolomics analysis revealed that, as expected, BMDM were not highly metabolically active, with few metabolites up- or downregulated from unstimulated to the CAM-activated state. Therefore, in cells with little FA metabolism, it was difficult to detect a large FATP1-mediated effect. In the absence of *Fatp1*, the PPP was upregulated, suggesting that FATP1 normally acts to limits MΦ ROS production through the PPP. The PPP is a source of the NADPH required for iNOS generation of ROS. Another source of oxidative stress in CAM-activated MΦs is the shunting of arginine to iNOS, which catalyzes the conversion of arginine to NO. AAM-activated MΦs divert arginine instead to *arginase-1*, which converts arginine to ornithine. Ornithine, a precursor of collagen synthesis, is necessary for AAM function in tissue remodeling and wound repair [4]. Thus, in AAMs, less arginine is directed towards iNOS and, therefore, production of ROS and collateral tissue oxidative damage is reduced. Herein, the combined result of enhanced PPP and iNOS activity in the absence of *Fatp1* is ROS production and oxidative damage to tissues. Indeed, oxidative damage evident in HFD-exposed adipose from $Fatp1^{B-/-}$ mice further supported metabolic shifts linked to increased ROS production in the absence of *Fatp1*. Additionally, one metabolite greatly regulated by loss of *Fatp1* in BMDM was riboflavin (Vitamin B2). Riboflavin is a central component of the cofactors flavin mononucleotide (FMN) and flavin adenine dinucleotide (FAD) and is necessary for many flavoprotein enzyme reactions including oxidases including the phagocytic NADPH oxidase 2 (Nox2), Complex I and Complex II of the electron transport chain, Vitamin B6 and B3 production, as well as oxidation of pyruvate, α-ketoglutarate, branched-chain amino acids, and fatty acids. In addition, reduction of the oxidized form of glutathione (GSSG) to its reduced form (GSH) by glutathione reductase is FAD dependent. Thus, a host of metabolically relevant pathways are regulated by riboflavin. Interestingly, *Fatp1* toggled riboflavin concentrations: unstimulated BMDM lacking *Fatp1* had almost two-fold greater riboflavin while CAM stimulated $Fatp1^{B-/-}$ contained just a third of control levels. In MΦs, riboflavin has been shown to reduce oxidative burst, immune response, and resistance to infection [85,86]. Taken together, the complex regulation of metabolites such as riboflavin in unstimulated and stimulated states suggests that detailed time course studies are necessary to fully establish the contribution of FATP1 to riboflavin-mediated inflammation.

In contrast to BMDM, RAW MΦs were very metabolically active with tens to hundreds of metabolites differentially regulated in the unstimulated or CAM-activated state. RAW cells are an immortalized and rapidly proliferating cell line, which is reflected in the metabolic profile. Hence, there were greater *Fatp1*-dependent differences detected in the RAW cells compared to BMDM, likely because of needs for membrane synthesis during proliferation and other processes. RAW MΦs did not express detectable FATP1 protein, which emphasizes the importance of this model as a gain of function approach. FATP1 overexpression elevated ACSL activity and fatty acid uptake, as well as the concentration of many fatty acids demonstrating the profound capacity of this transporter to alter MΦ lipid composition. Compared to *Fatp1*-deficient MΦs, the opposite shift in substrate metabolism was observed in RAW MΦs over-expressing FATP1: FATP1 overexpression suppressed *Glut1*, glucose uptake, glycolytic rate and capacity, and glucose oxidation. However, similar to the "mixed" M1/M2 phenotype commonly detected *in vivo*, the metabolic phenotype of FATP1-OE RAW MΦs is also a mixture of what was traditionally considered

CAM-like and AAM-like metabolism. We find that, despite a dramatic down-regulation of glycolysis using bioenergetics analysis, metabolomics analysis also revealed decreased intermediates of the TCA cycle, potentially supporting a more energetic phenotype in that the cells are relying upon other substrates in oxidative metabolism [75,87,88]. Detailed flux analysis is warranted to further study the impact of FATP1 on glycolysis and oxidative metabolism.

In conjunction with reduced glycolysis, CAM-like RAW MΦs overexpressing FATP1 failed to be fully CAM activated: Fatp1 overexpression reduced CAM-stimulated iNOS, TNFα, IL-6, MCP1 and IL-1β, while it almost tripled Hmox-1. Metabolomic analysis supported that FATP1 overexpression blunted induction of iNOS activity in response to CAM activation as evidenced by more than a 50% reduction in citrulline and an increase in polyamines and polyamine associated metabolites (which demonstrated a redirection of arginine from iNOS metabolism towards arginase-1 metabolism). *Hmox-1* catalyzes the degradation of heme, thus protecting against iron-induced oxidative damage [56] and was reduced in *Fatp1*$^{-/-}$ BMDM. Since RAW MΦs are originally derived from viral-induced mouse leukemia and display a Warburg-like metabolism reminiscent of the CAM-like phenotype, the inhibition of pro-inflammatory activation by the metabolic switch induced by FATP1 was striking, although we did not observe an increase in alternatively activated markers including Mrc1 or Arg1, reiterating the importance of specific fatty acid transporters in metabolic reprogramming.

FATP1 is assigned to the "negative regulation of phospholipid biosynthetic process" gene ontology class based on the study from Mitchell et al. [89]. Metabolomics data indicated enhanced glycerolipid metabolism in the absence of *Fatp1*, with increases observed in ethanolamine, glycerophosphocholine, and CDP-choline in CAM activated *Fatp1*$^{-/-}$ BMDM. Phospholipids serve as a pool of bioactive lipids including arachidonic, linoleic, and palmitic acid, which could modulate MΦ-mediated inflammation [90]. Therefore, future studies will determine if FATP1 regulates MΦ activation via regulation of ratios of phospholipid classes and/or fatty acid composition within those classes. Metabolomic evidence demonstrated potent regulation of long chain fatty acids arachidonate and linoleate, sources of bioactive lipid mediators including eicosanoids. Eicosanoids have stimulatory and inhibitory effects, are short-lived, and are often further metabolized to lipid mediators that may have activities far extending the precursor. FATP1 overexpression greatly decreased availability of one of the main eicosanoid precursors, free arachidonate, to almost undetectable levels. In line with altered substrate availability, FATP1 overexpression greatly reduced arachidonate-derived HETE metabolites and some linoleate-derived eicosanoids such as 9,10-DHOME. 15-HETE was increased in *Fatp1*$^{-/-}$ BMDM, supporting a critical reciprocal role for FATP1 gain and loss of activity in some eicosanoid production. HETEs are formed by the 5-, 12- and 15-lipoxygenase (LO) pathways. 5- and 12-LO products are mainly pro-inflammatory [91], whereas the main 15-LO product 15-HETE has anti-inflammatory capacities, although evidence exists that 15-HETE also induces ROS production [92]. Interestingly, the diol 9,10-diHOME is implicated as a cytotoxic agent [93]. Importantly, oxidation of many eicosanoids is an NAD + -dependent process (e.g. 15-hydroxyprostaglandin dehydrogenase), thus the production of eicosanoids is directly responsive to mitochondrial metabolism. Furthermore, one lipid-derived metabolite

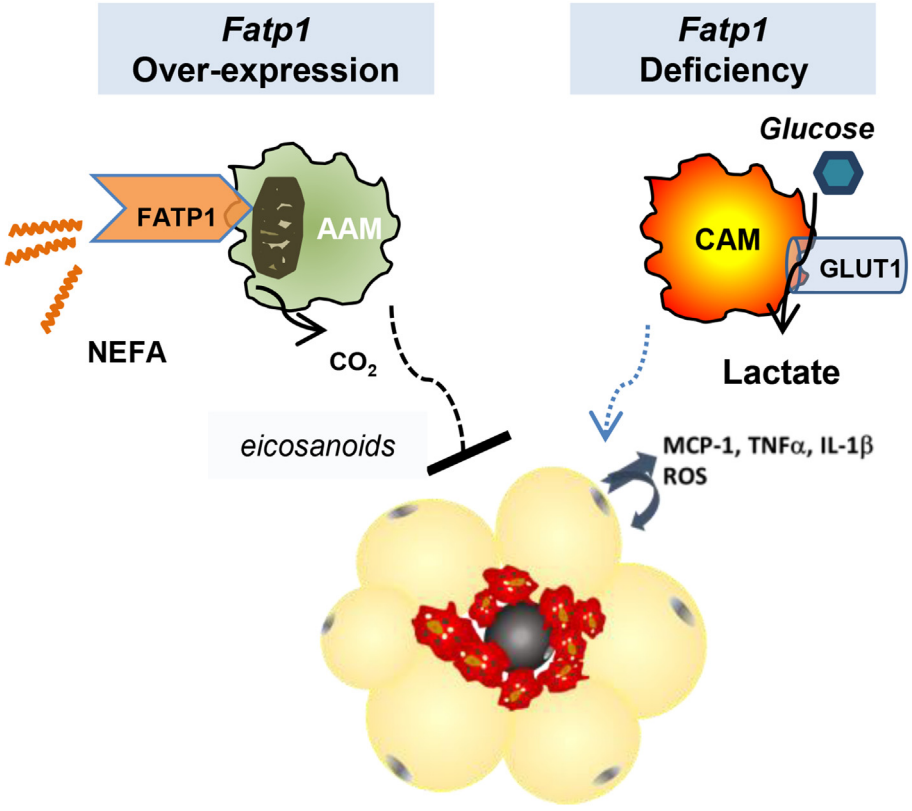

Figure 6: FATP1 is a novel regulator of immunometabolism: Working Model: Fatty acid transport protein (FATP1) is necessary to maintain the alternatively activated macrophage (AAM) phenotype, limit oxidative stress, and to reduce high fat diet (HFD)-induced adipose tissue inflammation and systemic glucose intolerance. Deficiency of *Fatp1* exacerbates classic macrophage (CAM) activation and HFD-induced metabolic dysfunction.

dramatically upregulated by FATP1 overexpression was 9-HODE, a PPARγ agonist derived from linoleic acid [94]. Activation of PPARγ is well-known to reduce inflammation and could be a potential mechanism through which FATP1 may function to limit inflammation. Thus, FATP1 may regulate ROS and inflammation through activation of long chain fatty acid precursors to modulate production of eicosanoids, combined with modulation of mitochondrial metabolism. While an attempt was made to measure eicosanoids in white adipose tissue, any MΦ-specific effects were surely masked by the sheer lipid mass of the tissue. Therefore, ATM-specific eicosanoid analysis is necessary. Further radiotracer, flux analysis, and inhibitor or loss-of-function studies are also necessary to fully comprehend the complexity of FATP1's role in lipid mediator biology.

Finally, we have begun to examine FATP1's effects in a translational approach. *Fatp1* contains genetic variants (i.e. single nucleotide polymorphisms, SNPs) associated with diabetes or risk factors for diabetes [95,96]. Variants located in and near *FATP1* were detected that were associated with *FATP1* expression in human adipose tissue. *Fatp1* is upregulated by adiponectin, PPARγ, and the orphan receptor TR4, therefore, the interaction between variants and transcriptional regulation of *Fatp1* expression should be further studied. While encouraging, these findings were detected at the tissue level in *total* subcutaneous adipose tissue. Hence, it was impossible to take into account the complexity of the cellular composition of the adipose microenvironment and effects specifically on ATMs. Indeed, few large population genetic studies focus solely on monocyte/MΦs and future genetic analysis of this immune population is of great interest.

5. CONCLUSION

In summary, integrating loss- and gain-of-function models, we report for the first time that MΦ FATP1 is necessary to elicit the AAM phenotype *in vitro* and controls MΦ activation and adipose inflammation *in vivo* (see model in Figure 6). We present mechanistic insight into the relationship between FATP1 and inflammation, a previously unrecognized regulator of MΦ substrate metabolism and inflammation. MΦs are an extremely heterogeneous population of cells whose capacity for metabolic flexibility has important implications for local and systemic responses to diet and other insults. Our investigation into preferential metabolic substrate usage by MΦs has demonstrated that FATP1 is a novel regulator of immunometabolism. While this project focused on metabolic changes in the macrophage and the resulting *in vitro* and *in vivo* consequences, there are many questions left unanswered including FATP1's role in phagocytosis, antigen presentation, motility, as well as interactions with other key cells such as T cells important to metabolic diseases.

8. ACKNOWLEDGMENTS

We thank E. Klett for assessment of pancreata morphology, L.O. Li for technical assistance on ACSL assays, and H. Wen for advice regarding the inflammasome. This work was supported by National Institutes of Health (NIH) grants F32HL75970 (A.R.J), P30DK056350 (J.J.M., J.A.G., L.M.), Z01ES025034 (M.L.E., D.C.Z.), DK034987 (J.A.G.), DK099311 (P.T.F.), R01CA096500 (B.D.), DK089202 and DK101293 (A.S.), AA017376 (L.M.), UNC undergraduate research fellowship (M.J.H.), Sanofi Global Scholar pre-doctoral fellowship (Y.Q.), UNC Chancellor's Fellowship (A.J.C.), American Heart Association 1-14-BS-191 (A.S.), American Heart Association (L.M.) and UNC University Cancer Research Fund (L.M.). The METSIM adipose study was supported by the Academy of Finland (contract 124243), the Finnish Heart Foundation, the Finnish Diabetes Foundation, Tekes contract 1510/31/06, the Commission of the European Community (HEALTH-F2-2007-201681) and US NIH grants DK093757, DK072193, DK062370 and 1Z01 HG000024 (KM).

CONFLICT OF INTEREST

The authors have declared that no conflict of interest exists.

APPENDIX A. SUPPLEMENTARY DATA

Supplementary data related to this article can be found at http://dx.doi.org/10.1016/j.molmet.2016.04.005.

REFERENCES

[1] Weisberg, S.P., McCann, D., Desai, M., Rosenbaum, M., Leibel, R.L., Ferrante Jr., A.W., 2003. Obesity is associated with macrophage accumulation in adipose tissue. Journal of Clinical Investigation 112(12):1796–1808. PubMed PMID: 14679176.

[2] Trayhurn, P., 2013. Hypoxia and adipose tissue function and dysfunction in obesity. Physiological Reviews 93(1):1–21. http://dx.doi.org/10.1152/physrev.00017.2012. Epub 2013/01/11. PubMed PMID: 23303904.

[3] Sundaram, S., Johnson, A.R., Makowski, L., 2013. Obesity, metabolism and the microenvironment: links to cancer. Journal of Carcinogenesis 12:19. http://dx.doi.org/10.4103/1477-3163.119606. Epub 2013/11/15. PubMed PMID: 24227994; PubMed Central PMCID: PMC3816318.

[4] Johnson, A.R., Milner, J.J., Makowski, L., 2012. The inflammation highway: metabolism accelerates inflammatory traffic in obesity. Immunologic Reviews 249(1):218–238. Epub May 2012.

[5] Devevre, E.F., Renovato-Martins, M., Clement, K., Sautes-Fridman, C., Cremer, I., Poitou, C., 2015. Profiling of the three circulating monocyte subpopulations in human obesity. Journal of Immunology 194(8):3917–3923. http://dx.doi.org/10.4049/jimmunol.1402655. Epub 2015/03/20. PubMed PMID: 25786686.

[6] Gordon, S., 2007. The macrophage: past, present and future. European Journal of Immunology 37(Suppl. 1):S9–S17. http://dx.doi.org/10.1002/eji.200737638. Epub 2007/11/01. PubMed PMID: 17972350.

[7] Fain, J.N., 2010. Release of inflammatory mediators by human adipose tissue is enhanced in obesity and primarily by the nonfat cells: a review. Mediators of Inflammation 2010:513948. http://dx.doi.org/10.1155/2010/513948. Epub 2010/05/29. PubMed PMID: 20508843; PubMed Central PMCID: PMC2874930.

[8] Shoelson, S.E., Lee, J., Goldfine, A.B., 2006. Inflammation and insulin resistance. Journal of Clinical Investigation 116(7):1793–1801. http://dx.doi.org/10.1172/JCI29069. Epub 2006/07/11. PubMed PMID: 16823477; PubMed Central PMCID: PMC1483173.

[9] Kadl, A., Meher, A.K., Sharma, P.R., Lee, M.Y., Doran, A.C., Johnstone, S.R., et al., 2010. Identification of a novel macrophage phenotype that develops in response to atherogenic phospholipids via Nrf2. Circulation Research 107(6):737–746. http://dx.doi.org/10.1161/CIRCRESAHA.109.215715. Epub 2010/07/24. PubMed PMID: 20651288; PubMed Central PMCID: PMC2941538.

[10] Kratz, M., Coats, B.R., Hisert, K.B., Hagman, D., Mutskov, V., Peris, E., et al., 2014. Metabolic dysfunction drives a mechanistically distinct proinflammatory phenotype in adipose tissue macrophages. Cell Metabolism 20(4):614–625. http://dx.doi.org/10.1016/j.cmet.2014.08.010. Epub 2014/09/23. PubMed PMID: 25242226; PubMed Central PMCID: PMC4192131.

[11] Xu, X., Grijalva, A., Skowronski, A., van Eijk, M., Serlie, M.J., Ferrante Jr., A.W., 2013. Obesity activates a program of lysosomal-dependent lipid metabolism in adipose tissue macrophages independently of classic activation. Cell Metabolism 18(6):816–830. http://dx.doi.org/10.1016/

j.cmet.2013.11.001. Epub 2013/12/10. PubMed PMID: 24315368; PubMed Central PMCID: PMC3939841.

[12] Huang, S.C., Everts, B., Ivanova, Y., O'Sullivan, D., Nascimento, M., Smith, A.M., et al., 2014. Cell-intrinsic lysosomal lipolysis is essential for alternative activation of macrophages. Nature Immunology 15(9):846–855. http://dx.doi.org/10.1038/ni. 2956. Epub 2014/08/05. PubMed PMID: 25086775; PubMed Central PMCID: PMC4139419.

[13] O'Neill, L.A., Pearce, E.J., 2016. Immunometabolism governs dendritic cell and macrophage function. The Journal of Experimental Medicine 213(1):15–23. http://dx.doi.org/10.1084/jem.20151570. Epub 2015/12/24. PubMed PMID: 26694970; PubMed Central PMCID: PMC4710204.

[14] Gautier, E.L., Shay, T., Miller, J., Greter, M., Jakubzick, C., Ivanov, S., et al., 2012. Gene-expression profiles and transcriptional regulatory pathways that underlie the identity and diversity of mouse tissue macrophages. Nature Immunology 13(11):1118–1128. http://dx.doi.org/10.1038/ni. 2419. Epub 2012/10/02. PubMed PMID: 23023392; PubMed Central PMCID: PMC3558276.

[15] Jha, A.K., Huang, S.C., Sergushichev, A., Lampropoulou, V., Ivanova, Y., Loginicheva, E., et al., 2015. Network integration of parallel metabolic and transcriptional data reveals metabolic modules that regulate macrophage polarization. Immunity 42(3):419–430. http://dx.doi.org/10.1016/j.immuni.2015.02.005. Epub 2015/03/19. PubMed PMID: 25786174.

[16] Tannahill, G.M., Curtis, A.M., Adamik, J., Palsson-McDermott, E.M., McGettrick, A.F., Goel, G., et al., 2013. Succinate is an inflammatory signal that induces IL-1beta through HIF-1alpha. Nature 496(7444):238–242. http://dx.doi.org/10.1038/nature11986. Epub 2013/03/29. PubMed PMID: 23535595.

[17] Freemerman, A.J., Johnson, A.R., Sacks, G.N., Milner, J.J., Kirk, E.L., Troester, M.A., et al., 2014. Metabolic reprogramming of macrophages: glucose transporter 1 (GLUT1)-mediated glucose metabolism drives a pro-inflammatory phenotype. The Journal of Biological Chemistry 289(11): 7884–7896. http://dx.doi.org/10.1074/jbc.M113.522037. Epub 2014/02/05. PubMed PMID: 24492615; PubMed Central PMCID: PMC3953299.

[18] Vats, D., Mukundan, L., Odegaard, J.I., Zhang, L., Smith, K.L., Morel, C.R., et al., 2006. Oxidative metabolism and PGC-1beta attenuate macrophage-mediated inflammation. Cell Metabolism 4(1):13–24. PubMed PMID: 16814729.

[19] Haschemi, A., Kosma, P., Gille, L., Evans, C.R., Burant, C.F., Starkl, P., et al., 2012. The sedoheptulose kinase CARKL directs macrophage polarization through control of glucose metabolism. Cell Metabolism 15(6):813–826. http://dx.doi.org/10.1016/j.cmet.2012.04.023. Epub 2012/06/12. PubMed PMID: 22682222; PubMed Central PMCID: PMC3370649.

[20] Sundaram, S., Freemerman, A.J., Galanko, J.A., McNaughton, K.K., Bendt, K.M., Darr, D.B., et al., 2014. Obesity-mediated regulation of HGF/c-Met is associated with reduced basal-like breast cancer latency in parous mice. PLoS One 9(10):e111394. http://dx.doi.org/10.1371/journal.pone.0111394. Epub 2014/10/30. PubMed PMID: 25354395; PubMed Central PMCID: PMC4213021.

[21] Aouadi, M., Vangala, P., Yawe, J.C., Tencerova, M., Nicoloro, S.M., Cohen, J.L., et al., 2014. Lipid storage by adipose tissue macrophages regulates systemic glucose tolerance. American Journal of Physiology, Endocrinology & Metabolism 307(4):E374–E383. http://dx.doi.org/10.1152/ajpendo.00187.2014. Epub 2014/07/06. PubMed PMID: 24986598; PubMed Central PMCID: PMC4137117.

[22] Nomura, M., Liu, J., Rovira II, , Gonzalez-Hurtado, E., Lee, J., Wolfgang, M.J., et al., 2016. Fatty acid oxidation in macrophage polarization. Nature Immunology 17(3):216–217. http://dx.doi.org/10.1038/ni. 3366. Epub 2016/02/18. PubMed PMID: 26882249.

[23] Everts, B., Amiel, E., van der Windt, G.J., Freitas, T.C., Chott, R., Yarasheski, K.E., et al., 2012. Commitment to glycolysis sustains survival of NO-producing inflammatory dendritic cells. Blood 120(7):1422–1431. http://dx.doi.org/10.1182/blood-2012-03-419747. Epub 2012/07/13. PubMed PMID: 22786879; PubMed Central PMCID: PMC3423780.

[24] Hall, A.M., Smith, A.J., Bernlohr, D.A., 2003. Characterization of the Acyl-CoA synthetase activity of purified murine fatty acid transport protein 1. Journal of Biological Chemistry 278(44):43008–43013. http://dx.doi.org/10.1074/jbc.M306575200. Epub 2003/08/26. PubMed PMID: 12937175.

[25] Baillie, A.G., Coburn, C.T., Abumrad, N.A., 1996. Reversible binding of long-chain fatty acids to purified FAT, the adipose CD36 homolog. Journal of Membrane Biology 153(1):75–81. PubMed PMID: 8694909.

[26] Hirsch, D., Stahl, A., Lodish, H.F., 1998. A family of fatty acid transporters conserved from mycobacterium to man. Proceedings of the National Academy of Sciences of the United States of America 95(15):8625–8629. Epub 1998/07/22. PubMed PMID: 9671728; PubMed Central PMCID: PMC21126.

[27] Binnert, C., Koistinen, H.A., Martin, G., Andreelli, F., Ebeling, P., Koivisto, V.A., et al., 2000. Fatty acid transport protein-1 mRNA expression in skeletal muscle and in adipose tissue in humans. American Journal of Physiology Endocrinology and Metabolism 279(5):E1072–E1079. Epub 2000/10/29. PubMed PMID: 11052962.

[28] Guitart, M., Osorio-Conles, O., Pentinat, T., Cebria, J., Garcia-Villoria, J., Sala, D., et al., 2014. Fatty acid transport protein 1 (FATP1) localizes in mitochondria in mouse skeletal muscle and regulates lipid and ketone body disposal. PLoS One 9(5):e98109. http://dx.doi.org/10.1371/journal.pone.0098109. Epub 2014/05/27. PubMed PMID: 24858472; PubMed Central PMCID: PMC4032244.

[29] Wu, Q., Ortegon, A.M., Tsang, B., Doege, H., Feingold, K.R., Stahl, A., 2006. FATP1 is an insulin-sensitive fatty acid transporter involved in diet-induced obesity. Molecular Cell Biology 26(9):3455–3467. http://dx.doi.org/10.1128/MCB.26.9.3455–3467.2006 [pii] 26/9/3455. Epub 2006/04/14. PubMed PMID: 16611988; PubMed Central PMCID: PMC1447434.

[30] Kim, J.K., Gimeno, R.E., Higashimori, T., Kim, H.J., Choi, H., Punreddy, S., et al., 2004. Inactivation of fatty acid transport protein 1 prevents fat-induced insulin resistance in skeletal muscle. Journal of Clinical Investigation 113(5): 756–763. http://dx.doi.org/10.1172/JCI18917. Epub 2004/03/03. PubMed PMID: 14991074; PubMed Central PMCID: PMC351314.

[31] Stahl, A., Evans, J.G., Pattel, S., Hirsch, D., Lodish, H.F., 2002. Insulin causes fatty acid transport protein translocation and enhanced fatty acid uptake in adipocytes. Developmental Cell 2(4):477–488 doi: S1534580702001430 [pii]. Epub 2002/04/24. PubMed PMID: 11970897.

[32] Liu, Q., Gauthier, M.S., Sun, L., Ruderman, N., Lodish, H., 2010. Activation of AMP-activated protein kinase signaling pathway by adiponectin and insulin in mouse adipocytes: requirement of acyl-CoA synthetases FATP1 and Acsl1 and association with an elevation in AMP/ATP ratio. FASEB Journal 24(11):4229–4239. http://dx.doi.org/10.1096/fj.10-159723 [pii] fj.10-159723. Epub 2010/07/30. PubMed PMID: 20667975; PubMed Central PMCID: PMC2974418.

[33] Xu, N., Zhang, S.O., Cole, R.A., McKinney, S.A., Guo, F., Haas, J.T., et al., 2012. The FATP1-DGAT2 complex facilitates lipid droplet expansion at the ER-lipid droplet interface. The Journal of Cell Biology 198(5):895–911. http://dx.doi.org/10.1083/jcb.201201139. Epub 2012/08/29. PubMed PMID: 22927462; PubMed Central PMCID: PMC3432760.

[34] Zhan, T., Poppelreuther, M., Ehehalt, R., Fullekrug, J., 2012. Overexpressed FATP1, ACSVL4/FATP4 and ACSL1 increase the cellular fatty acid uptake of 3T3-L1 adipocytes but are localized on intracellular membranes. PLoS One 7(9):e45087. http://dx.doi.org/10.1371/journal.pone.0045087. Epub 2012/10/02. PubMed PMID: 23024797; PubMed Central PMCID: PMC3443241.

[35] https://www.immgen.org/.

[36] Stahl, A., Hirsch, D.J., Gimeno, R.E., Punreddy, S., Ge, P., Watson, N., et al., 1999. Identification of the major intestinal fatty acid transport protein. Molecular Cell 4(3):299–308. Epub 1999/10/13. PubMed PMID: 10518211.

[37] Sundaram, S., Freemerman, A.J., Johnson, A.R., Milner, J.J., McNaughton, K.K., Galanko, J.A., et al., 2013. Role of HGF in obesity-associated tumorigenesis: C3(1)-TAg mice as a model for human basal-like

breast cancer. Breast Cancer Research and Treatment 142(3):489–503. http://dx.doi.org/10.1007/s10549-013-2741-5. Epub 2013/11/13. PubMed PMID: 24218051; PubMed Central PMCID: PMC3904507.

[38] Li, L.O., Mashek, D.G., An, J., Doughman, S.D., Newgard, C.B., Coleman, R.A., 2006. Overexpression of rat long chain acyl-coa synthetase 1 alters fatty acid metabolism in rat primary hepatocytes. Journal of Biological Chemistry 281(48):37246–37255. http://dx.doi.org/10.1074/jbc.M604427200. Epub 2006/10/10. PubMed PMID: 17028193.

[39] Bhatt, A.P., Jacobs, S.R., Freemerman, A.J., Makowski, L., Rathmell, J.C., Dittmer, D.P., et al., 2012. Dysregulation of fatty acid synthesis and glycolysis in non-Hodgkin lymphoma. Proceedings of National Academy of Sciences United States of America 109(29):11818–11823. http://dx.doi.org/10.1073/pnas.1205995109. Epub 2012/07/04. PubMed PMID: 22752304; PubMed Central PMCID: PMC3406848.

[40] Edin, M.L., Wang, Z., Bradbury, J.A., Graves, J.P., Lih, F.B., DeGraff, L.M., et al., 2011. Endothelial expression of human cytochrome P450 epoxygenase CYP2C8 increases susceptibility to ischemia-reperfusion injury in isolated mouse heart. FASEB Journal: Official Publication of the Federation of American Societies for Experimental Biology 25(10):3436–3447. http://dx.doi.org/10.1096/fj.11-188300. Epub 2011/06/24. PubMed PMID: 21697548; PubMed Central PMCID: PMC3177568.

[41] Makowski, L., Boord, J.B., Maeda, K., Babaev, V.R., Uysal, K.T., Morgan, M.A., et al., 2001. Lack of macrophage fatty-acid-binding protein aP2 protects mice deficient in apolipoprotein E against atherosclerosis. Nature Medicine 7(6):699–705. PubMed PMID: 11385507.

[42] Furuhashi, M., Fucho, R., Gorgun, C.Z., Tuncman, G., Cao, H., Hotamisligil, G.S., 2008. Adipocyte/macrophage fatty acid-binding proteins contribute to metabolic deterioration through actions in both macrophages and adipocytes in mice. Journal of Clinical Investigation 118(7):2640–2650. PubMed PMID: 18551191.

[43] Holman, R.R.H.G., Kennedy, I., Stevens, R.J., Matthews, D., Levy, J.C., 2004. A calculator for HOMA. Diabetologia 47(Suppl. 1:A222).

[44] Murphy, A.J., Akhtari, M., Tolani, S., Pagler, T., Bijl, N., Kuo, C.L., et al., 2011. ApoE regulates hematopoietic stem cell proliferation, monocytosis, and monocyte accumulation in atherosclerotic lesions in mice. The Journal of Clinical Investigation 121(10):4138–4149. http://dx.doi.org/10.1172/JCI57559. Epub 2011/10/05. PubMed PMID: 21968112; PubMed Central PMCID: PMC3195472.

[45] Qin, Y., Hamilton, J.L., Bird, M.D., Chen, M.M., Ramirez, L., Zahs, A., et al., 2013. Adipose inflammation and macrophage infiltration after binge ethanol and burn injury. Alcoholism, Clinical and Experimental Research. http://dx.doi.org/10.1111/acer.12210. Epub 2013/08/06. PubMed PMID: 23909743.

[46] Sampey, B.P., Vanhoose, A.M., Winfield, H.M., Freemerman, A.J., Muehlbauer, M.J., Fueger, P.T., et al., 2011. Cafeteria diet is a robust model of human metabolic syndrome with liver and adipose inflammation: comparison to high-fat diet. Obesity (Silver Spring) 19(6):1109–1117. http://dx.doi.org/10.1038/oby.2011.18. Epub 2011/02/19. PubMed PMID: 21331068; PubMed Central PMCID: PMC3130193.

[47] Chen, Y.C., Colvin, E.S., Maier, B.F., Mirmira, R.G., Fueger, P.T., 2013. Mitogen-inducible gene 6 triggers apoptosis and exacerbates ER stress-induced beta-cell death. Molecular Endocrinology 27(1):162–171. http://dx.doi.org/10.1210/me.2012-1174. Epub 2012/12/04. PubMed PMID: 23204325; PubMed Central PMCID: PMC3545216.

[48] Othy, S., Bruneval, P., Topcu, S., Dugail, I., Delers, F., Lacroix-Desmazes, S., et al., 2012. Effect of IVIg on human dendritic cell-mediated antigen uptake and presentation: role of lipid accumulation. Journal of Autoimmunity 39(3):168–172. http://dx.doi.org/10.1016/j.jaut.2012.05.013. Epub 2012/06/19. PubMed PMID: 22704540.

[49] Milner, J.J., Sheridan, P.A., Karlsson, E.A., Schultz-Cherry, S., Shi, Q., Beck, M.A., 2013. Diet-induced obese mice exhibit altered heterologous immunity during a secondary 2009 pandemic H1N1 infection. Journal of Immunology 191(5):2474–2485. http://dx.doi.org/10.4049/jimmunol.1202429. Epub 2013/08/02. PubMed PMID: 23904168; PubMed Central PMCID: PMC3756476.

[50] Schenkel, L.C., Singh, R.K., Michel, V., Zeisel, S.H., da Costa, K.A., Johnson, A.R., et al., 2014. Mechanism of choline deficiency and membrane alteration in postural orthostatic tachycardia syndrome primary skin fibroblasts. FASEB Journal: Official Publication of the Federation of American Societies for Experimental Biology. http://dx.doi.org/10.1096/fj.14-258566. Epub 2014/12/04. PubMed PMID: 25466896.

[51] Grundberg, E., Small, K.S., Hedman, A.K., Nica, A.C., Buil, A., Keildson, S., et al., 2012. Multiple tissue human expression resource C. mapping cis- and trans-regulatory effects across multiple tissues in twins. Nature Genetics 44(10):1084–1089. http://dx.doi.org/10.1038/ng. 2394. Epub 2012/09/04. PubMed PMID: 22941192; PubMed Central PMCID: PMC3784328.

[52] Mahendran, Y., Vangipurapu, J., Cederberg, H., Stancakova, A., Pihlajamaki, J., Soininen, P., et al., 2013. Association of ketone body levels with hyperglycemia and type 2 diabetes in 9,398 Finnish men. Diabetes 62(10):3618–3626. http://dx.doi.org/10.2337/db12-1363. Epub 2013/04/06. PubMed PMID: 23557707; PubMed Central PMCID: PMC3781437.

[53] Stegle, O., Parts, L., Piipari, M., Winn, J., Durbin, R., 2012. Using probabilistic estimation of expression residuals (PEER) to obtain increased power and interpretability of gene expression analyses. Nature Protocols 7(3):500–507. http://dx.doi.org/10.1038/nprot.2011.457. Epub 2012/02/22. PubMed PMID: 22343431; PubMed Central PMCID: PMC3398141.

[54] Wu, C., Orozco, C., Boyer, J., Leglise, M., Goodale, J., Batalov, S., et al., 2009. BioGPS: an extensible and customizable portal for querying and organizing gene annotation resources. Genome Biology 10(11):R130. http://dx.doi.org/10.1186/gb-2009-10-11-r130. PubMed PMID.

[55] Abraham, N.G., Junge, J.M., Drummond, G.S., 2015. Translational significance of heme oxygenase in obesity and metabolic syndrome. Trends in Pharmacological Sciences. http://dx.doi.org/10.1016/j.tips.2015.09.003. Epub 2015/10/31. PubMed PMID: 26515032.

[56] Corna, G., Campana, L., Pignatti, E., Castiglioni, A., Tagliafico, E., Bosurgi, L., et al., 2010. Polarization dictates iron handling by inflammatory and alternatively activated macrophages. Haematologica 95(11):1814–1822. http://dx.doi.org/10.3324/haematol.2010.023879. Epub 2010/06/01. PubMed PMID: 20511666; PubMed Central PMCID: PMC2966902.

[57] Maeda, K., Cao, H., Kono, K., Gorgun, C.Z., Furuhashi, M., Uysal, K.T., et al., 2005. Adipocyte/macrophage fatty acid binding proteins control integrated metabolic responses in obesity and diabetes. Cell Metabolism 1(2):107–119. PubMed PMID: 16054052.

[58] Orr, J.S., Puglisi, M.J., Ellacott, K.L., Lumeng, C.N., Wasserman, D.H., Hasty, A.H., 2012. Toll-like receptor 4 deficiency promotes the alternative activation of adipose tissue macrophages. Diabetes 61(11):2718–2727. http://dx.doi.org/10.2337/db11-1595. Epub 2012/07/04. PubMed PMID: 22751700; PubMed Central PMCID: PMC3478520.

[59] Wen, H., Miao, E.A., Ting, J.P., 2013. Mechanisms of NOD-like receptor-associated inflammasome activation. Immunity 39(3):432–441. http://dx.doi.org/10.1016/j.immuni.2013.08.037. Epub 2013/09/24. PubMed PMID: 24054327; PubMed Central PMCID: PMC3835203.

[60] Baardman, J., Licht, I., de Winther, M.P., Van den Bossche, J., 2015. Metabolic-epigenetic crosstalk in macrophage activation. Epigenomics 7(7):1155–1164. http://dx.doi.org/10.2217/epi.15.71. Epub 2015/11/21. PubMed PMID: 26585710.

[61] Cheng, S.C., Quintin, J., Cramer, R.A., Shepardson, K.M., Saeed, S., Kumar, V., et al., 2014. mTOR- and HIF-1alpha-mediated aerobic glycolysis as metabolic basis for trained immunity. Science 345(6204):1250684. http://dx.doi.org/10.1126/science.1250684. Epub 2014/09/27. PubMed PMID: 25258083; PubMed Central PMCID: PMC4226238.

[62] Saeed, S., Quintin, J., Kerstens, H.H., Rao, N.A., Aghajanirefah, A., Matarese, F., et al., 2014. Epigenetic programming of monocyte-to-

macrophage differentiation and trained innate immunity. Science 345(6204): 1251086. http://dx.doi.org/10.1126/science.1251086. Epub 2014/09/27. PubMed PMID: 25258085; PubMed Central PMCID: PMC4242194.

[63] Ogden, C.L., Carroll, M.D., Flegal, K.M., 2014. Prevalence of obesity in the United States. JAMA 312(2):189–190. http://dx.doi.org/10.1001/jama.2014.6228. Epub 2014/07/10. PubMed PMID: 25005661.

[64] Donath, M.Y., 2014. Targeting inflammation in the treatment of type 2 diabetes: time to start. Nature Reviews Drug Discovery 13(6):465–476. http://dx.doi.org/10.1038/nrd4275. Epub 2014/05/24. PubMed PMID: 24854413.

[65] Boni-Schnetzler, M., Donath, M.Y., 2013. How biologics targeting the IL-1 system are being considered for the treatment of type 2 diabetes. British Journal of Clinical Pharmacology 76(2):263–268. http://dx.doi.org/10.1111/j.1365-2125.2012.04297.x. Epub 2012/04/18. PubMed PMID: 22506644; PubMed Central PMCID: PMC3731600.

[66] Hanefeld, M., Pistrosch, F., Koehler, C., Chiasson, J.L., 2012. Conversion of IGT to type 2 diabetes mellitus is associated with incident cases of hypertension: a post-hoc analysis of the STOP-NIDDM trial. Journal of Hypertension 30(7):1440–1443. http://dx.doi.org/10.1097/HJH.0b013e328354663c. Epub 2012/05/11. PubMed PMID: 22573126.

[67] Stanley, T.L., Zanni, M.V., Johnsen, S., Rasheed, S., Makimura, H., Lee, H., et al., 2011. TNF-alpha antagonism with etanercept decreases glucose and increases the proportion of high molecular weight adiponectin in obese subjects with features of the metabolic syndrome. Journal of Clinical Endocrinology and Metabolism 96(1):E146–E150. http://dx.doi.org/10.1210/jc.2010-1170. Epub 2010/11/05. PubMed PMID: 21047923; PubMed Central PMCID: PMC3038481.

[68] Solomon, D.H., Massarotti, E., Garg, R., Liu, J., Canning, C., Schneeweiss, S., 2011. Association between disease-modifying antirheumatic drugs and diabetes risk in patients with rheumatoid arthritis and psoriasis. JAMA 305(24): 2525–2531. http://dx.doi.org/10.1001/jama.2011.878. Epub 2011/06/23. PubMed PMID: 21693740.

[69] Antohe, J.L., Bili, A., Sartorius, J.A., Kirchner, H.L., Morris, S.J., Dancea, S., et al., 2012. Diabetes mellitus risk in rheumatoid arthritis: reduced incidence with anti-tumor necrosis factor alpha therapy. Arthritis Care & Research 64(2): 215–221. http://dx.doi.org/10.1002/acr.20657. Epub 2011/10/06. PubMed PMID: 21972198.

[70] Lackey, D.E., Olefsky, J.M., 2016. Regulation of metabolism by the innate immune system. Nature Reviews Endocrinology 12(1):15–28. http://dx.doi.org/10.1038/nrendo.2015.189. Epub 2015/11/11. PubMed PMID: 26553134.

[71] Erbay, E., Cao, H., Hotamisligil, G.S., 2007. Adipocyte/macrophage fatty acid binding proteins in metabolic syndrome. Current Atherosclerosis Reports 9(3): 222–229. Epub 2008/02/05. PubMed PMID: 18241617.

[72] Makowski, L., Brittingham, K.C., Reynolds, J.M., Suttles, J., Hotamisligil, G.S., 2005. The fatty acid-binding protein, aP2, coordinates macrophage cholesterol trafficking and inflammatory activity. Macrophage expression of aP2 impacts peroxisome proliferator-activated receptor gamma and IkappaB kinase activities. Journal of Biological Chemistry 280(13):12888–12895. PubMed PMID: 15684432.

[73] Makowski, L., Hotamisligil, G.S., 2005. The role of fatty acid binding proteins in metabolic syndrome and atherosclerosis. Current Opinion in Lipidology 16(5):543–548. PubMed PMID: 16148539.

[74] Kanter, J.E., Kramer, F., Barnhart, S., Averill, M.M., Vivekanandan-Giri, A., Vickery, T., et al., 2012. Diabetes promotes an inflammatory macrophage phenotype and atherosclerosis through acyl-CoA synthetase 1. Proceedings of National Academy Sciences United States of America 109(12):E715–E724. http://dx.doi.org/10.1073/pnas.1111600109. Epub 2012/02/07. PubMed PMID: 22308341; PubMed Central PMCID: PMC3311324.

[75] Kramer, P.A., Ravi, S., Chacko, B., Johnson, M.S., Darley-Usmar, V.M., 2014. A review of the mitochondrial and glycolytic metabolism in human platelets and leukocytes: implications for their use as bioenergetic biomarkers. Redox Biology 2:206–210. http://dx.doi.org/10.1016/j.redox.2013.12.026. Epub 2014/02/05. PubMed PMID: 24494194; PubMed Central PMCID: PMC3909784.

[76] Wen, H., Ting, J.P., O'Neill, L.A., 2012. A role for the NLRP3 inflammasome in metabolic diseases—did Warburg miss inflammation? Nature Immunology 13(4):352–357 http://dx.doi.org/10.1038/ni. 2228. Epub 2012/03/21. PubMed PMID: 22430788.

[77] Han, C.Y., Umemoto, T., Omer, M., Den Hartigh, L.J., Chiba, T., Leboeuf, R., et al., 2012. NADPH oxidase-derived reactive oxygen species increases expression of monocyte chemotactic factor genes in cultured adipocytes. Journal of Biological Chemistry 287(13):10379–10393. http://dx.doi.org/10.1074/jbc.M111.304998. Epub 2012/01/31. PubMed PMID: 22287546; PubMed Central PMCID: PMC3322984.

[78] Johnson, A.R., Wilkerson, M.D., Sampey, B.P., Troester, M.A., Hayes, D.N., Makowski, L., 2016. Cafeteria diet-induced obesity causes oxidative damage in white adipose. Biochemical and Biophysical Research Communications. http://dx.doi.org/10.1016/j.bbrc.2016.03.113. Epub 2016/04/02. PubMed PMID: 27033600.

[79] Mashima, R., Nakanishi-Ueda, T., Yamamoto, Y., 2003. Simultaneous determination of methionine sulfoxide and methionine in blood plasma using gas chromatography-mass spectrometry. Analytical Biochemistry 313(1):28–33. Epub 2003/02/11. PubMed PMID: 12576054.

[80] Wang, T.J., Ngo, D., Psychogios, N., Dejam, A., Larson, M.G., Vasan, R.S., et al., 2013. 2-Aminoadipic acid is a biomarker for diabetes risk. The Journal of Clinical Investigation 123(10):4309–4317. http://dx.doi.org/10.1172/JCI64801. Epub 2013/10/05. PubMed PMID: 24091325; PubMed Central PMCID: PMC3784523.

[81] Zeitoun-Ghandour, S., Leszczyszyn, O.I., Blindauer, C.A., Geier, F.M., Bundy, J.G., Sturzenbaum, S.R., 2011. *C. elegans* metallothioneins: response to and defence against ROS toxicity. Molecular Biosystems 7(8):2397–2406. http://dx.doi.org/10.1039/c1mb05114h. Epub 2011/06/08. PubMed PMID: 21647514.

[82] Wijekoon, E.P., Skinner, C., Brosnan, M.E., Brosnan, J.T., 2004. Amino acid metabolism in the Zucker diabetic fatty rat: effects of insulin resistance and of type 2 diabetes. Canadian Journal of Physiology and Pharmacology 82(7): 506–514. http://dx.doi.org/10.1139/y04-067. Epub 2004/09/25. PubMed PMID: 15389298.

[83] Yuan, W., Zhang, J., Li, S., Edwards, J.L., 2011. Amine metabolomics of hyperglycemic endothelial cells using capillary LC-MS with isobaric tagging. Journal of Proteome Research 10(11):5242–5250. http://dx.doi.org/10.1021/pr200815c. Epub 2011/10/04. PubMed PMID: 21961526.

[84] Reynaert, N.L., Ckless, K., Guala, A.S., Wouters, E.F., van der Vliet, A., Janssen-Heininger, Y.M., 2006. In situ detection of S-glutathionylated proteins following glutaredoxin-1 catalyzed cysteine derivatization. Biochimica et Biophysica Acta 1760(3):380–387. http://dx.doi.org/10.1016/j.bbagen.2006.01.006. Epub 2006/03/07. PubMed PMID: 16515838.

[85] Schramm, M., Wiegmann, K., Schramm, S., Gluschko, A., Herb, M., Utermohlen, O., et al., 2014. Riboflavin (vitamin B2) deficiency impairs NADPH oxidase 2 (Nox2) priming and defense against *Listeria monocytogenes*. European Journal of Immunology 44(3):728–741. http://dx.doi.org/10.1002/eji.201343940. Epub 2013/11/26. PubMed PMID: 24272050.

[86] Mazur-Bialy, A.I., Buchala, B., Plytycz, B., 2013. Riboflavin deprivation inhibits macrophage viability and activity – a study on the RAW 264.7 cell line. The British Journal of Nutrition 110(3):509–514. http://dx.doi.org/10.1017/S0007114512005351. Epub 2013/02/19. PubMed PMID: 23415257.

[87] Ganeshan, K., Chawla, A., 2014. Metabolic regulation of immune responses. Annual Review of Immunology 32:609–634. http://dx.doi.org/10.1146/annurev-immunol-032713-120236. Epub 2014/03/25. PubMed PMID: 24655299.

[88] Buck, M.D., O'Sullivan, D., Pearce, E.L., 2015. T cell metabolism drives immunity. Journal of Experimental Medicine 212(9):1345–1360. http://dx.doi.org/10.1084/jem.20151159. Epub 2015/08/12. PubMed PMID: 26261266; PubMed Central PMCID: PMC4548052.

[89] Mitchell, R.W., Hatch, G.M., 2009. Regulation of cardiolipin biosynthesis by fatty acid transport protein-1 IN HEK 293 cells. Biochimica et Biophysica Acta 1788(10):2015–2021. http://dx.doi.org/10.1016/j.bbamem.2009.06.002. Epub 2009/06/16. PubMed PMID: 19523918.

[90] Balsinde, J., Balboa, M.A., Dennis, E.A., 1997. Inflammatory activation of arachidonic acid signaling in murine P388D1 macrophages via sphingomyelin synthesis. The Journal of Biological Chemistry 272(33):20373–20377. Epub 1997/08/15. PubMed PMID: 9252342.

[91] Clark, S.R., Guy, C.J., Scurr, M.J., Taylor, P.R., Kift-Morgan, A.P., Hammond, V.J., et al., 2011. Esterified eicosanoids are acutely generated by 5-lipoxygenase in primary human neutrophils and in human and murine infection. Blood 117(6):2033–2043. http://dx.doi.org/10.1182/blood-2010-04-278887. Epub 2010/12/24. PubMed PMID: 21177434; PubMed Central PMCID: PMC3374621.

[92] Mahipal, S.V., Subhashini, J., Reddy, M.C., Reddy, M.M., Anilkumar, K., Roy, K.R., et al., 2007. Effect of 15-lipoxygenase metabolites, 15-(S)-HPETE and 15-(S)-HETE on chronic myelogenous leukemia cell line K-562: reactive oxygen species (ROS) mediate caspase-dependent apoptosis. Biochemical Pharmacology 74(2):202–214. http://dx.doi.org/10.1016/j.bcp.2007.04.005. Epub 2007/05/23. PubMed PMID: 17517376.

[93] Moran, J.H., Weise, R., Schnellmann, R.G., Freeman, J.P., Grant, D.F., 1997. Cytotoxicity of linoleic acid diols to renal proximal tubular cells. Toxicology and Applied Pharmacology 146(1):53–59. http://dx.doi.org/10.1006/taap.1997.8197. Epub 1997/09/23. PubMed PMID: 9299596.

[94] Nagy, L., Tontonoz, P., Alvarez, J.G., Chen, H., Evans, R.M., 1998. Oxidized LDL regulates macrophage gene expression through ligand activation of PPARgamma. Cell 93(2):229–240. Epub 1998/05/06. PubMed PMID: 9568715.

[95] Gertow, K., Skoglund-Andersson, C., Eriksson, P., Boquist, S., Orth-Gomer, K., Schenck-Gustafsson, K., et al., 2003. A common polymorphism in the fatty acid transport protein-1 gene associated with elevated post-prandial lipaemia and alterations in LDL particle size distribution. Atherosclerosis 167(2):265–273. Epub 2003/06/24. PubMed PMID: 12818409.

[96] Meirhaeghe, A., Martin, G., Nemoto, M., Deeb, S., Cottel, D., Auwerx, J., et al., 2000. Intronic polymorphism in the fatty acid transport protein 1 gene is associated with increased plasma triglyceride levels in a French population. Arteriosclerosis, Thrombosis and Vascular Biology 20(5):1330–1334. Epub 2000/05/16. PubMed PMID: 10807750.

